

# 1 Sensitivity of black carbon concentrations and climate impact to 2 aging and scavenging in OsloCTM2-M7

---

3 Marianne T. Lund<sup>1,\*</sup>, Terje K. Berntsen<sup>1,2</sup>, Bjørn H. Samset<sup>1</sup>

4

5 *1 CICERO - Center for International Climate and Environmental Research, Oslo, Norway*

6 *2 Department of Geosciences, University of Oslo, Oslo, Norway*

7 *\*Corresponding author, [m.t.lund@cicero.oslo.no](mailto:m.t.lund@cicero.oslo.no), Phone: +47 22 85 86 94*

## 8 **Abstract**

9 Accurate representation of black carbon (BC) concentrations in climate models is a key  
10 prerequisite for understanding its net climate impact. BC aging scavenging are treated very  
11 differently in present models. Here, we examine the sensitivity of 3-dimensional, temporally  
12 resolved BC concentrations to perturbations to individual model processes in the chemistry-  
13 transport model OsloCTM2-M7. The main goals are to identify processes related to aerosol  
14 aging and scavenging where additional observational constraints may most effectively improve  
15 model performance, in particular for BC vertical profiles, and to give an indication of how  
16 model uncertainties in the BC life cycle propagate into uncertainties in climate impacts.  
17 Coupling OsloCTM2 with the microphysical aerosol module M7 allows us to investigate aging  
18 processes in more detail than possible with a simpler bulk parameterization. Here we include,  
19 for the first time in this model, a treatment of condensation of nitric acid on BC. Using radiative  
20 kernels, we also estimate the range of radiative forcing and global surface temperature  
21 responses that may result from perturbations to key tunable parameters in the model. We find  
22 that BC concentrations in OsloCTM2-M7 are particularly sensitive to convective scavenging  
23 and the inclusion of condensation by nitric acid. The largest changes are found at higher  
24 altitudes around the Equator and at low altitudes over the Arctic. Convective scavenging of  
25 hydrophobic BC, and the amount of sulfate required for BC aging, are found to be key  
26 parameters, potentially reducing bias against HIPPO flight-based measurements by 60 to 90  
27 percent. Even for extensive tuning, however, the total impact on global mean surface  
28 temperature is estimated to less than 0.04K. Similar results are found when nitric acid is allowed  
29 to condense on the BC aerosols. We conclude, in line with previous studies, that a shorter  
30 atmospheric BC lifetime broadly improves the comparison with measurements over the Pacific.  
31 However, we also find that the model-measurement discrepancies can not be uniquely attributed

32 to uncertainties in a single process or parameter. Model development therefore needs to be  
33 focused on improvements to individual processes, supported by a broad range of observational  
34 and experimental data, rather than tuning of individual, effective parameters such as the global  
35 BC lifetime.

36

## 37 **1 Introduction**

38 Black carbon (BC) aerosols play an important role in the climate system through several  
39 mechanisms including direct absorption of solar radiation (Bond et al., 2013; Myhre et al.,  
40 2013), changing surface albedo (Flanner et al., 2009; Warren & Wiscombe, 1980), modification  
41 of cloud properties and thermal stability (Koch & Del Genio, 2010; Lohmann & Feichter, 2005),  
42 and influence on precipitation and circulation (Bollasina et al., 2014; Wang et al., 2015). The  
43 potentially strong climate warming, combined with short atmospheric residence time and  
44 harmful health impacts (Anenberg et al., 2012; Aunan et al., 2006; Shindell et al., 2011), has  
45 made BC reductions an attractive mitigation measure (AMAP, 2015; Bowerman et al., 2013;  
46 EPA, 2012; Grieshop et al., 2009; Kopp & Mauzerall, 2010; UNEP/WMO, 2011).

47

48 Modeling atmospheric concentrations of BC remains challenging. In particular, it has been well  
49 documented that the current model ensembles do not accurately reproduce measured BC  
50 vertical profiles (e.g., (Koch et al., 2009b; Lee et al., 2013; Samset et al., 2014; Schwarz et al.,  
51 2013; Wang et al., 2014)). Additionally, global models often underestimate Arctic BC surface  
52 concentrations and fail to capture the seasonal cycle (e.g., Eckhardt et al. (2015); Shindell et al.  
53 (2008)). Because the radiative forcing (RF) and temperature response to a perturbation in BC  
54 depends strongly on altitude, such discrepancies propagate to uncertainties in the net BC climate  
55 impact. For instance, overestimating high-altitude BC concentrations can result in an  
56 overestimation of the subsequent RF (Samset & Myhre, 2011), while too low surface  
57 concentrations may lead to an underestimation of the temperature response due to the reduced  
58 efficacy of BC forcing with altitude (Ban-Weiss et al., 2011; Flanner, 2013; Samset & Myhre,  
59 2015). This in turn poses significant challenges for the design and evaluation of effective BC  
60 mitigation strategies. Studies have shown that both modeled global vertical BC profiles and the  
61 transport of the aerosols to the Arctic is strongly influenced by the parameterization of  
62 scavenging and aging (Allen & Landuyt, 2014; Bourgeois & Bey, 2011; Browse et al., 2012;  
63 Fan et al., 2012; Kipling et al., 2016). However, these parameterizations differ considerably

64 between current models. Increasing the understanding of factors controlling the distribution of  
65 BC in different global atmospheric and climate models is therefore essential.

66  
67 Here we examine the sensitivity of modeled BC concentrations to factors controlling aerosol  
68 lifetime in the OsloCTM2 (Sovde et al., 2008) coupled with the aerosol microphysical  
69 parameterization M7 (Vignati et al., 2004) (hereafter OsloCTM2-M7). The chemical transport  
70 model OsloCTM2 has been documented and used in several multi-model aerosol studies  
71 (Balkanski et al., 2010; Myhre et al., 2013; Schulz et al., 2006; Shindell et al., 2013; Textor et  
72 al., 2007). These studies used a simplified bulk aerosol scheme. Lund and Berntsen (2012)  
73 (hereafter LB12) performed the first analysis of BC simulated by the M7 in the OsloCTM2 and  
74 compared results with those from the bulk parameterization. A basic evaluation against selected  
75 measurements was performed, showing that using M7 improved the representation of Arctic  
76 surface concentrations compared with the bulk scheme, but exacerbated the overestimation of  
77 high-altitude BC.

78  
79 Building on the findings in LB12, we perform a range of sensitivity experiments varying key  
80 assumptions in the treatment of aging and scavenging in OsloCTM2-M7 and investigate the  
81 resulting range in vertical BC profiles, as well as high-latitude surface concentrations. Using  
82 updated emission inventories, three years of model results and observations from surface  
83 stations, flight campaigns, and snow samples, we also perform a more thorough documentation  
84 of the current model performance. Our experiments include a first step towards accounting for  
85 BC aging by gas-phase nitric acid condensation. Measurements have shown that nitrate is  
86 frequently present in internal aerosol mixtures (Pratt & Prather, 2010; Shiraiwa et al., 2007).  
87 Aging through interaction with nitrate may also become more important in the future following  
88 strong projected decreases in SO<sub>2</sub> emissions and increasing NO<sub>x</sub> and greenhouse gas emissions  
89 (Bauer et al., 2007; Bellouin et al., 2011; Makkonen et al., 2012), but has so far not been  
90 accounted for in the model. We also take the analysis one step further and estimate the range in  
91 global RF and surface temperature resulting from the changes in the model parameters. The  
92 model setup and experiments are described in Sect. 2, results presented and discussed in Sect.  
93 3 and conclusions given in Sect. 4

94  
95  
96

## 97 **2 Methodology**

### 98 *2.1 The OsloCTM2-M7*

99 The OsloCTM2 is a global off-line 3-dimensional chemistry transport model with transport  
100 driven by meteorological data generated by the Integrated Forecast System (IFS) model at the  
101 European Center for Medium Range Weather Forecast (ECMWF) (Sovde et al., 2008). The  
102 model is run for 2008-2010 with a T42 resolution (approximately 2.8° x 2.8°) and 60 vertical  
103 layers from the surface to 0.1 hPa.

104

105 The microphysical aerosol module M7 (Vignati et al., 2004) includes sea salt, mineral dust,  
106 sulfate and organic carbon, in addition to BC. Aerosols are represented by seven modes with  
107 size distribution given by a lognormal distribution function. BC exists in the Aitken soluble  
108 (mixed) and insoluble mode, soluble accumulation and soluble coarse modes. All BC is emitted  
109 in the insoluble Aitken mode upon emission. Aging and growth subsequently occurs due to  
110 condensation of sulfuric acid produced in the gas-phase oxidation reaction of SO<sub>2</sub> by  
111 OH+SO<sub>2</sub>→H<sub>2</sub>SO<sub>4</sub> and coagulation with soluble particles. See LB12 for additional details.

112 Wet deposition in OsloCTM2-M7 is calculated based on ECMWF data for convective activity,  
113 cloud fraction and rain fall, and on the solubility of individual species. Removal in large-scale  
114 cloud systems follow the scheme by Berge (1993), (Berglen et al., 2004) The parameterization  
115 of deep convection is based on the Tiedtke mass flux scheme (Tiedtke, 1989), with mass  
116 redistributed in the vertical by a so-called “elevator” principle, i.e., surplus or deficit of mass in  
117 the column (Berglen et al., 2004). BC Pparticles in the soluble modes are assumed to be  
118 hygroscopic and are removed according to the fraction of the liquid plus ice water content of a  
119 cloud that is removed by precipitation (Berntsen et al., 2006). In the baseline setup, assuming  
120 100% scavenging efficiency (i.e., solubility) by both water and ice in both large-scale and by  
121 convective precipitation is assumed in the baseline setup. The model does not account for sub-  
122 cloud scavenging. Since LB12, the temporal frequency of wet scavenging in OsloCTM2-M7  
123 has been reduced from three to one hour. The OsloCTM2-M7 also keeps track of the BC  
124 deposition and concentration in snow; see Appendix A of Skeie et al. (2011) for description.  
125 Dry deposition in the OsloCTM2-M7 follows Wesely (1989), with a modification for species  
126 in the M7 to include size-dependent dry deposition velocities following Seinfeld and Pandis  
127 (1998).

128 The M7 is coupled to the sulfur/oxidant chemistry in OsloCTM2-M7. Nitrate is not included in  
129 the baseline M7 setup. However, we perform a sensitivity experiment where gaseous nitric acid

130 is allowed to condense on insoluble BC particles and contribute to aging (Sect. 2.3). The sulfate  
131 and nitrate modules in the model are described in detail in Berglen et al. (2004) and Myhre et  
132 al. (2006), and we only give brief summaries here.

133 The sulfur cycle chemistry scheme includes dimethyl sulfide (DMS), SO<sub>2</sub>, sulfate, H<sub>2</sub>S and  
134 methane sulfonic acid (MSA) and the concentrations of sulfur is calculated interactively with  
135 the oxidant chemistry. Sulfate is formed by gas-phase and aqueous-phase oxidation of SO<sub>2</sub> by  
136 OH, H<sub>2</sub>O<sub>2</sub>, HO<sub>2</sub>NO<sub>2</sub> and O<sub>3</sub>. When M7 is used, the gas-phase sulfate is saved in a separate  
137 tracer and allowed to condense on the insoluble aerosol modes. The aqueous phase sulfate is  
138 distributed to the accumulation and coarse mode sulfate tracers in M7 according to a prescribed  
139 fraction. The treatment of sulfate aerosols then follows M7.

140 ~~The chemical equilibrium between of semi-volatile-inorganic species is simulated~~ treated with  
141 the Equilibrium Simplified Aerosol model (EQSAM) (Metzger et al., 2002a; Metzger et al.,  
142 2002b). EQSAM considers the NH<sub>4</sub><sup>+</sup>/Na<sup>+</sup>/SO<sub>4</sub><sup>2-</sup>/NO<sub>3</sub><sup>-</sup>/Cl<sup>-</sup>/H<sub>2</sub>O system and ~~and calculates the~~  
143 ~~gas/aerosol partitioning of ammonium nitrate under the assumption that the~~ aerosols are  
144 assumed to be metastable, internally mixed and obey thermodynamic gas/aerosol equilibrium.  
145 Based on the ammonium to sulfate ratio, EQSAM first calculates the preferred state of sulfate.  
146 Excess ammonia is available to partition to the aerosol phase, together with gaseous nitric acid,  
147 as described in Myhre et al. (2006). Emissions of ammonia are described in Sect. 2.2, while  
148 nitric acid is produced through photochemistry as described in Berntsen and Isaksen (1997).  
149 The Nitrate and ammonium aerosols isare represented by two modes, a fine mode comprised  
150 of sulfate and a coarse mode comprised of sea salt, and gaseous ammonia and nitric acid can  
151 condense on any of these. After H<sub>2</sub>SO<sub>4</sub> and nitric acid have been generated by the  
152 photochemistry, the thermodynamic equilibrium is solved using EQSAM.

## 153 *2.2 Emissions*

154 Anthropogenic emissions for 2008-2010 are from the ECLIPSEv4 inventory (Klimont et al.,  
155 2016) ~~developed with the GAINS model (Amman et al. 2011) as part of the activities under the~~  
156 ~~ECLIPSE project funded by the European Commission 7<sup>th</sup> Framework~~ (available upon request  
157 from <http://eclipse.nilu.no/>). Emissions from international shipping and aviation are from the  
158 Representative Concentration Pathway (RCP) 6.0 (Fujino et al., 2006; Hijioka et al., 2008).  
159 Biomass burning emissions are from the Global Fire Emission Database version 3 (GFEDv3)  
160 (van der Werf et al., 2010), biogenic emissions from MEGAN2.1 (Guenther et al., 2012) and  
161 natural emissions of ammonia from GEIA (Bouwman et al., 1997). Seasonal variability in

162 domestic emissions is accounted for by using monthly weights (2000-2006 average) for each  
163 grid based on spatially distributed temperature data from the Climate Research Unit (CRU)  
164 following the methodology described in Streets et al. (2003), while seasonality in agricultural  
165 waste burning is obtained from GFEDv3. Seasonality of emissions in other sectors is not  
166 included in ECLIPSEv4. ~~In the more recently released ECLIPSEv5 inventory (), the monthly~~  
167 ~~variability in emissions from other sectors is small or negligible.~~ Total BC emissions in 2010  
168 are 5866 Gg from fossil fuel plus biofuel sources and 2273 Gg from biomass burning.

### 169 *2.3 Experiments*

170 We first perform a three-year base simulation with meteorological data and emissions for 2008-  
171 2010, which forms the basis for the model evaluation. Next, we perform a range of sensitivity  
172 experiments described in the following paragraphs and summarized in Table 1.

173  
174 Several sensitivity experiments are related to the aging of BC. First, we explore the impact of  
175 varying the amount of soluble material (i.e., sulfate from gas-phase oxidation of SO<sub>2</sub>) required  
176 to transfer the BC aerosols to the soluble mode. The M7 uses the concept of monolayers (ML);  
177 when sufficient soluble material is associated with a hydrophobic particle to form “n”  
178 monomolecular layers around the particle, the particle is assumed hygroscopic and is  
179 transferred to the mixed mode. The amount of soluble material required for a particle to become  
180 hygroscopic is an important source of uncertainty (Vignati et al., 2010). Popovicheva et al.  
181 (2011) used a laboratory approach to quantify the water uptake by particles with varying  
182 amounts of sulfates in order to simulate the aging of combustion particles. Based on a  
183 quantification measure for separating hygroscopic and non-hygroscopic soots (Popovicheva et  
184 al., 2008), the laboratory results suggest that the transformation of soot particles from  
185 hydrophobic to hydrophilic requires an H<sub>2</sub>SO<sub>4</sub> surface coverage of 0.5-1.4 ML, while 1.4-2.3  
186 ML were required for transformation to hygroscopic mode. Based on these results we perform  
187 three model simulations where the ML requirement is changed from 1 in the baseline to 0.5,  
188 1.4 and 2.3, respectively. Next, we perform a test where 50% of BC from biomass burning  
189 sources is emitted directly in the accumulation mode instead of in the insoluble Aitken mode.  
190 This is based on observational evidence suggesting that biomass burning BC tends to be larger  
191 and more aged, with thicker coatings than BC from urban source (Schwarz et al., 2008). Finally,  
192 we test the impact of allowing for BC aging by condensation of gas-phase nitric acid. We extend  
193 M7, in a simplified manner, to also account for condensation by nitric acid on insoluble particles  
194 after gas/aerosol partitioning ~~with ammonium nitrate~~ is calculated in EQSAM. In this

195 experiment, nitric acid contributes only to the transfer of BC from insoluble to soluble Aitken  
196 mode, with no further impact on aerosol size distribution. We follow the same treatment of  
197 condensation as for sulfate in M7 (Vignati et al., 2004) and adopt an accommodation coefficient  
198 for nitric acid of 0.1 (Pringle et al., 2010). The number of MLs used as the criterion for aging  
199 ranges in existing literature. In its original setup M7 assumes 1 ML, based on the best agreement  
200 with a sectional model found by Vignati et al. (2004), but this considers sulfate as the only  
201 condensable species. Other studies have used a 5 (Pringle et al., 2010) and 10 (Mann et al.,  
202 2010) monolayer scheme. Reflecting this range and examining the subsequent impact on  
203 concentrations, we here perform three runs assuming 1, 5 and 10 ML are required for aging.

204  
205 The second set of sensitivity experiments is related to wet scavenging, the main loss mechanism  
206 of BC and thus a key parameter for the lifetime and distribution. Hydrophilic BC is originally  
207 assumed to be 100% removed by both liquid and ice in large-scale mixed-phase clouds in the  
208 OsloCTM2-M7. However, this high efficiency of BC removal by ice-phase precipitation is  
209 uncertain. Koch et al. (2009a) found that assuming 12% ice removal of BC gave optimal  
210 agreement with observations. This fraction was also supported by observations in Cozic et al.  
211 (2007) and has been adopted in studies with the OsloCTM2 bulk aerosol parameterization (e.g.,  
212 Skeie et al. (2011)). Here we compare results with 100% and 12% removal efficiency for large-  
213 scale ice-phase clouds. The removal scheme in OsloCTM2-M7 also assumes no wet scavenging  
214 of hydrophobic particles. However, hydrophobic BC aerosol may still be subject to removal by  
215 impact scavenging or act as ice nuclei (IN) in convective and mixed-phase clouds (Ekman et  
216 al., 2006; Kajino et al., 2012; Park et al., 2005). The BC IN activity is not well known. To  
217 represent some of this uncertainty, we perform two sensitivity experiments assuming either 100%  
218 or 20% removal efficiency of hydrophobic BC by convective precipitation, with the latter  
219 loosely based on Hoose et al. (2010). We also perform a combination experiment assuming 12%  
220 removal efficiency of hydrophilic BC by large-scale ice-phase clouds and 20% removal of  
221 hydrophobic BC by convective precipitation.

222  
223 Finally, we perform two additional tests to investigate the impact of seasonality in emissions  
224 and an increase in emissions in Russia following a recent study by Huang et al. (2015). We  
225 alternately remove the seasonal variation in domestic and agricultural waste burning emissions  
226 and replace ECLIPSEv4 emissions in Russia with the Huang et al. (2015) inventory. These  
227 experiments have limited impact on the global BC distributions, but their influence on the  
228 seasonal cycle of Arctic BC concentrations is discussed in Sect. 3.1.1.

229

230 **TABLE 1**

231 *2.4 Radiative forcing and temperature response calculations*

232 To estimate implications of the concentration changes in our experiments for the global BC  
233 climate impact, we use precalculated radiative forcing (RF) and surface temperature (TS)  
234 kernels derived with the CESM-CAM4 (Samset & Myhre, 2015). These 3-dimensional,  
235 temporally varying kernels were constructed by systematically applying a uniform BC burden  
236 to one model layer at a time, and calculating the resulting responses. Effective radiative forcing  
237 (ERF) was extracted from simulations with prescribed sea-surface temperatures, while  
238 temperature responses were taken from simulations with a slab ocean setup. As shown in  
239 Samset and Myhre (2015), it is possible to take a perturbation to the 3D concentration, multiply  
240 it with the kernels, and get an estimate for the resulting ERF and temperature change. However,  
241 because the BC perturbations were applied uniformly throughout a single model layer, the  
242 temperature response at each grid point will be due to both BC forcing exerted locally and to  
243 forcing in surrounding gridboxes. Combined with the strong altitudinal dependence of forcing  
244 and temperature response on the BC perturbation, in the present analysis, we therefore focus on  
245 global mean horizontally averaged vertical profiles and not on changes at the grid point level in  
246 the present analysis. For each experiment, the globally averaged vertical BC profile from the  
247 OsloCTM2-M7 is multiplied with the globally averaged vertical forcing and temperature  
248 change kernels, respectively. The prior averaging of the profiles has a small impact on the net  
249 RF estimates (<10%, except in two cases where the difference compared to using 3D kernels is  
250 20%) (see also Stjern et al. (2016) for a fuller discussion on this issue). We also estimate the  
251 Arctic average forcing and response to Arctic BC concentrations changes and briefly investigate  
252 the potential uncertainties in Arctic TS using this kernel-based approach due to influence from  
253 forcing exerted outside the region. The latter is done by using a kernel for the temperature  
254 response caused only by the local Arctic BC perturbation from Flanner (2013) (see Sect. 3.3).  
255 Stjern et al. (2016) The kernels are interpolated to the OsloCTM2-M7 resolution before use.  
256 Both direct and semi-direct effects due to aerosol-radiation interactions are included in the  
257 kernel response. In line with the nomenclature of the IPCC Fifth Assessment Report we  
258 hereafter refer to the net effect as ERF<sub>ari</sub> and the direct effect only as RF<sub>ari</sub>.

259 As discussed by Samset and Myhre (2015), CAM4 does not account for the absorption  
260 enhancement due to BC aging, resulting in a lower RF<sub>ari</sub> per BC burden than earlier studies,  
261 especially at higher altitudes (e.g., Samset and Myhre (2011)). The consequent temperature

262 response per unit BC may also be underestimated. However, here we focus on the changes from  
263 the baseline in each sensitivity experiment rather than absolute climate impacts.

264

## 265 *2.5 Observations*

266 Modeled concentrations are evaluated against measurements from surface stations, flight  
267 campaigns and snow samples.

268 Measured surface concentrations of BC, sulfate, nitrate, sulfur dioxide and nitric acid across  
269 North America are from the IMPROVE and CASTNET networks, while measurements across  
270 Europe and the rest of the world are from the EBAS and NOAA GMD databases. We also use  
271 measurements in China from Zhang et al. (2012) and Aerosol Mass Spectrometer (AMS)  
272 campaigns summarized in Zhang et al. (2007).

273 To evaluate the model performance we calculate the ~~correlation coefficient and the~~ mean  
274 normalized bias (MNB) ~~and root mean square error (RMSE). The MNB for each species is~~  
275 ~~given by Equation 1:~~

$$276 \quad \text{MNB} = \frac{1}{N} \sum \left( \frac{C_{mod} - C_{obs}}{C_{obs}} \right) \quad (1)$$

$$277 \quad \text{RMSE} = \sqrt{\frac{1}{N} \sum (C_{mod} - C_{obs})^2}$$

278 where  $C_{mod}$  and  $C_{obs}$  is modeled and observed concentration and  $N$  is the total number of  
279 observations.

280 Following the recommendations by Petzold et al. (2013) observational data is referred to as  
281 equivalent BC (EBC), refractory BC (rBC) or elemental carbon (EC) depending on whether  
282 measurements are derived from optical absorption methods, incandescence methods or methods  
283 that specify the carbon content in carbonaceous matter. To convert to BC concentrations we  
284 adopt a mass-absorption cross-section (MAC) of  $9.7 \text{ m}^2/\text{g}$  (Bond & Bergstrom, 2006), except  
285 for Alert and Zeppelin, where we use the station-specific MAC reported by Lee et al. (2013).

286 BC in snow is compared to snow sample measurements across the Arctic in 2008/2009 (Doherty  
287 et al., 2010) and across Northern China in 2010 and 2012 (Wang et al., 2013; Ye et al., 2012).  
288 In the latter case, model results for 2010 are used.

289 Vertical profiles of modeled BC is compared with measurements from several flight campaigns,  
290 including ARCPAC (Aerosol, Radiation, and Cloud Processes affecting Arctic Climate),  
291 ARCTAS (Arctic Research of the Composition of the Troposphere from Aircraft and Satellites),  
292 HIAPER Pole-to-Pole Observations (HIPPO) and A-FORCE (Aerosol Radiative Forcing in  
293 East Asia). During ARCPAC and ARCTAS, flights were made across Alaska and Canadian  
294 Arctic in spring and summer of 2008 (Brock et al., 2011; Jacob et al., 2010), while HIPPO  
295 measured atmospheric constituents along transects from approximately pole-to-pole over the  
296 Pacific Ocean during different seasons from 2009 to 2011 (Wofsy et al., 2011). The A-FORCE  
297 campaign sampled air masses around Japan in March-April 2009 (Oshima et al., 2012). Data  
298 from ARCPAC, ARCTAS and HIPPO is available online from  
299 [www.esrl.noaa.gov/csd/projects/arcpac/](http://www.esrl.noaa.gov/csd/projects/arcpac/), [www.air.larc.nasa.gov/missions/arctas/arctas.html](http://www.air.larc.nasa.gov/missions/arctas/arctas.html)  
300 and [hippo.ornl.gov/](http://hippo.ornl.gov/). Data from A-FORCE was provided by Professor Yutaka Kondo,  
301 University of Tokyo (personal communication). Model data is also compared with CO  
302 concentrations measured during the campaigns.

303 Model data is interpolated in time and space and extracted along the flight track. An average  
304 profile for each campaign and latitude band is calculated by averaging observations and model  
305 results in 100 hPa altitude bins (25 hPa for HIPPO data between 400 and 200 hPa). The HIPPO  
306 data is also separated into five latitude bands. To evaluate the model performance in each  
307 experiment, we calculate the MNB for each campaign following Eq. 1, where N is determined  
308 by the number of altitude and latitude bins.

309

## 310 **3 Results and discussion**

### 311 *3.1 Model evaluation*

312 Before examining the impact of our sensitivity experiments on BC distribution, the baseline  
313 performance of the OsloCTM2-M7 must be documented. While the main focus of this paper is  
314 BC, the evaluation is extended to include species relevant for the BC aging process, including  
315 sulfate and sulfur dioxide. We also look at the modeled CO distribution. CO is another product  
316 of incomplete combustion and therefore has many of the same emission sources as BC.  
317 However, due to the longer lifetime of CO a comparison with observations, in particular in the  
318 more remote regions mainly influenced by long-range transport, can give an indication of how  
319 well the model represents the atmospheric transport.

### 320 3.1.1 Surface concentrations

321 On annual mean (year 2008), the OsloCTM2-M7 underestimates BC surface concentrations in  
322 Europe, North America and China with an overall MNB of -0.55 (Fig. S1). The underestimation  
323 is largest for measurements in China. The model also underestimates annual mean surface  
324 concentrations of sulfate (MNB -0.45), while nitrate concentrations are in better agreement with  
325 measurements, with MNB of 0.08. The overestimation of sulfur dioxide surface concentrations  
326 (MNB of 0.70) may be due to too inefficient conversion to sulfate, which is supported by the  
327 underestimation of sulfate aerosols, and/or an overestimation of emissions. Also nitric acid  
328 concentrations in Europe and North America are overestimated (MNB 0.75).

329 Figure 1 shows monthly mean modeled BC and measured EBC surface concentrations averaged  
330 over 2008-2010. The model reproduces the magnitude relatively well at Mace Head, Cape Point,  
331 Trinidad Head, Barrow and Pallas, but fail to capture some features in the seasonal variation.  
332 Concentrations are also underestimated at Lulin, Hohenpeissenberg and Jungfraujoch during  
333 winter and spring.

### 334 **FIGURE 1**

335 Studies have found that models often struggle to capture the seasonal cycle and magnitude of  
336 measured high-latitude BC surface concentrations (e.g., Eckhardt et al. (2015); Shindell et al.  
337 (2008)). While there has been considerable progress and several current models capture high-  
338 latitude-the seasonality in high-latitude surface concentrations better than previous generations  
339 (Breider et al., 2014; Browse et al., 2012; Liu et al., 2011; Sharma et al., 2013), discrepancies  
340 remain and there is considerable inter-model variability in simulated Arctic atmospheric BC  
341 burdensproblems remain (Mahmood et al., 2016). This is also the case for the OsloCTM2-M7.  
342 LB12 showed that inclusion of aerosol microphysics significantly improved both magnitude  
343 and seasonality of Arctic BC. Here we find further improvements by the use of updated  
344 emissions, partly due to the inclusion of emissions from flaring, which is an important local  
345 Arctic source of BC (Stohl et al., 2013). However, the model still underestimates concentrations  
346 during spring. The seasonal variability in emissions is an important factor. Accounting for  
347 seasonality in domestic BC emissions in the ECLIPSEv4 inventory increases the burden of total  
348 fossil fuel plus biofuel BC north of 65°N by approximately 15% during winter and by 2% on  
349 annual average compared to assuming constant monthly emissions. Over the same region,  
350 including seasonality in agricultural waste burning results in a 2-3% higher total BC burden  
351 during spring. This is a relatively small increase, but agricultural waste burning contributes only

352 around 6% to total BC emissions north of 40°N on an annual basis. Another potentially  
353 important factor is missing or underestimated emission sources. A recent study by Huang et al.  
354 (2015) estimate total anthropogenic BC emissions in Russia of 224 Gg, about 40% higher than  
355 in the ECLIPSEv4 inventory. Replacing the ECLIPSEv4 with those from Huang et al. (2015)  
356 increases the modeled BC burden north of 65N by about 16% during fall, winter and early  
357 spring and 2-10% during summer. Another possibly underestimated emission source is open  
358 waste burning. Wiedinmyer et al. (2014) use year 2010 population data and estimate that 631  
359 Gg BC is emitted globally from open waste burning, nearly a factor 7 more than in the  
360 ECLIPSEv4 inventory. Moreover, they suggest that open waste burning may contribute 30-50%  
361 to total anthropogenic PM<sub>10</sub> emissions in Russia, from where the near-surface transport of BC  
362 to the Arctic is effective (Stohl, 2006). Underestimation of this emission source may thus  
363 contribute to the too low modeled Arctic BC concentrations.

364 The OsloCTM2-M7 underestimates BC concentrations in snow compared to measurements, ~~in~~  
365 particularly in Russia, ~~Svalbard~~ and the Canadian Arctic, as has also been seen in previous  
366 studies. ~~Here we find somewhat higher modeled concentrations than in previous studies~~(Lund  
367 & Berntsen, 2012; Skeie et al., 2011). In the present analysis we find higher modeled  
368 concentrations than LB12, on the order of 5-15 ng g<sup>-1</sup> over large areas north of 70°N, likely  
369 owing to the updated emission inventory and shorter model time step for precipitation. However,  
370 this increase is insufficient to compensate for the existing underestimation in the  
371 abovementioned regions. The model and measurements agree better for many of the snow  
372 samples taken in China.

373 Eckhardt et al. (2015) show that models, including the OsloCTM2, have similar difficulties  
374 capturing the seasonality in Arctic sulfate concentrations as they have for BC. For instance, the  
375 OsloCTM2-M7 underestimates sulfur dioxide during spring at Zeppeling, but overestimates  
376 concentrations during summer. Through the aging process, such problems add to the  
377 uncertainties in modeled BC.

378 The model captures measured CO concentrations in the Northern Hemisphere during summer  
379 (Fig. S2), but underestimates the magnitude during winter/spring, a feature that has been shown  
380 also for other models in previous studies (Emmons et al., 2015; Monks et al., 2015). In the  
381 Southern Hemisphere, the model generally reproduces the magnitude better, with a slight  
382 overestimation during winter/spring at several stations. The ability of the model to reproduce  
383 the seasonal cycle and magnitude of CO, in particular at remote Southern Hemispheric stations

384 that are mainly influenced by long-range transport, suggests that the model represents  
385 atmospheric transport reasonably well and points to other processes as the dominant source of  
386 uncertainty in the model.

387

### 388 *3.1.2 Vertical profiles*

389 Figure 2 shows modeled vertical BC profiles against measurements from aircraft campaigns.  
390 Compared to measurements from ARCPAC and ARCTAS spring the OsloCTM2-M7  
391 underestimates the magnitude of BC concentrations throughout the atmosphere (Fig. 2 p,r;  
392 MNB -0.8). However, the shape of the profile is reproduced reasonably well. During April 2008,  
393 when these campaigns were undertaken, there was unusually strong fire activity in Siberia and  
394 air masses were heavily influenced by biomass burning emissions (Brock et al., 2011; Jacob et  
395 al., 2010; Warneke et al., 2009). During several flights, the biomass burning plumes were  
396 specifically targeted. Possible explanations for the strong discrepancies could therefore be  
397 underestimation of the fire emissions or inaccurate representation of the plumes in the model.  
398 The model also underestimates the magnitude of CO concentrations during these two  
399 campaigns (Fig. S3 (p,r); MNB -0.3), but again captures the profile shape reasonably well,  
400 providing further indication that too low emissions could be an important reason for the  
401 discrepancy. The agreement is better for ARCTAS summer (Fig. 2q; MNB 0.05). The majority  
402 of flights during the ARCTAS summer campaign took place over Canada, where the fire  
403 activity was generally low that year. Moreover, our evaluation against monthly surface  
404 concentrations of BC suggest a generally better agreement at high latitudes during summer than  
405 spring (Sect. 3.1.1). This is not the case for CO (Fig. S3 q; MNB -0.4).

406 Measurements from HIPPO are separated into five latitude bands (Fig. 2 a-o). For most latitude  
407 bands and flights, there is reasonable agreement close to the surface. In the 60-80N latitude  
408 band, the model overestimates concentrations close to the surface during HIPPO1 and 2, but  
409 underestimates concentrations during HIPPO3. HIPPO3 was undertaken during spring and a  
410 similar underestimation was also seen in the modeled surface measurements at Barrow during  
411 this time of year (Fig. 1). The model typically fail to reproduce the layered structure of the  
412 measured vertical profiles. In particular, the high-altitude concentrations in tropics and the  
413 southern mid-latitudes are overestimated. It should be noted that there are substantial  
414 differences between the three HIPPO campaigns although they all cover the Pacific. A better  
415 model-measurement agreement is found for HIPPO3 than for HIPPO1 and 2 (MNB 1.1, 3.3

416 and 2.8, respectively). In contrast to BC, both the magnitude and shape of most vertical CO  
417 profiles compare well across all latitude bands (Fig. S3 a-o; MNB 0.1, -0.1, -0.09).

418 There is quite good agreement between measured and modeled BC during the A-FORCE  
419 campaign (Fig. 2 s; MNB -0.1), with model results falling within one standard deviation of the  
420 measured profile. The A-FORCE campaign was carried out downstream of nearby emission  
421 sources and the good agreement with observations suggests reasonable representation in the  
422 model of both emission magnitude in the region and the mixing with the free troposphere on  
423 timescales of a few days. In contrast, the HIPPO campaigns sampled older air masses, where  
424 loss processes have had more time to influence the distribution. The CO concentrations is  
425 underestimated during A-FORCE (Fig. S3 s; MNB -0.3).

426 Our overall findings are in line with other recent studies. The tendency to overestimate high  
427 altitude BC concentrations over the Pacific has been noted for several other model (Kipling et  
428 al., 2013; Samset et al., 2014; Schwarz et al., 2013; Wang et al., 2014). The vertical profiles  
429 from OsloCTM2-M7 also fall roughly within the range of the AeroCom Phase II models  
430 (Samset et al., 2014).

## 431 **FIGURE 2**

432

### 433 *3.2 Sensitivity of BC concentrations to changes in aging and scavenging*

434 This section discusses the changes in modeled BC concentrations in our experiments, and  
435 examines the resulting range in vertical profiles and Arctic surface concentrations.

436 Table 2 summarizes the global BC burden and lifetime in each experiment. The global mean  
437 burden (lifetime) is 133 Gg (6 days) in the base simulation, while there is considerable range  
438 from 81 Gg (3.6 days) to about 185 Gg (8 days) across the experiments. The largest changes  
439 result from increasing the number of MLs required for aging (CoatThick2.3), allowing  
440 convective scavenging of hydrophobic BC (ConvBCi) and including aging by nitric acid  
441 (NitCond). The range of BC lifetimes still falls within that of estimates from different global  
442 models (e.g., Samset et al. (2014)).

## 443 **TABLE 2**

## 444 **FIGURE 3**

445 To examine the impacts in more detail, we calculate the differences in zonal mean concentration  
446 (Fig. 3) and burden (Fig. S45) between each experiment and the baseline. Figure S4 a shows  
447 the zonal mean concentration in the baseline simulation. The changes follow a similar spatial  
448 distribution in most all experiments, with largest changes in the lower model layers north of  
449 60°N and around the equatorial Atlantic. The changes in concentrations north of 60°N are  
450 largely determined by changes in the potential for long-range transport of BC from the northern  
451 hemisphere source regions with decreasing or increasing lifetime. The pronounced maxima  
452 over the equatorial Atlantic coincides with the outflow region with frequent precipitation from  
453 areas with high biomass burning activity, where changes in aging rate or lifetime strongly  
454 influences the amount that is removed by wet scavenging. In contrast to the other experiments,  
455 assuming that more biomass burning BC is emitted directly in the accumulation mode only has  
456 a very small effect on concentrations (Fig. 3 d). Asia is also an important BC source region;  
457 however, the absolute changes are smaller here than around the Equator. In the coating  
458 thickness experiments (Fig. 3 a-c), one possible explanation contributing to the differences  
459 could be sulfate levels, with higher concentrations available for coating of the BC particles, and  
460 thus lower sensitivity to changes in the aging requirement, in Asia.

461 ~~Not surprisingly, a~~Allowing for convective scavenging of hydrophobic BC results in  
462 considerable high-altitude changes, in particular over the tropics where convective activity is  
463 strong (Fig. 3 e,f). The maximum change in concentrations is shifted to northern mid-latitudes  
464 in the experiments when the large-scale ice scavenging efficiency of hydrophilic BC is reduced  
465 (Fig. 3 g,h), with the largest absolute changes over East Asia (Fig. S4 g,h). An increase in this  
466 region could reduce the general underestimation of surface concentrations found in the base  
467 simulation (Fig. S1). These experiments illustrate that the modeled concentrations are sensitive  
468 to the fractions of BC available for scavenging. For convective scavenging of hydrophobic  
469 aerosols, we assume either 20% or 100% to represent a wide range. However, the solubility and  
470 is parameter, and the BC-IN efficiency of BC, are uncertain parameters poorly constrained by  
471 observations.

472 The strong sensitivity of concentrations at high northern latitudes and around the tropics to  
473 changes in the convective scavenging of hydrophobic BC and inclusion of aging by nitric acid  
474 may seem surprising given that measurement suggest that significant the majority of freshly  
475 emitted hydrophobic BC particles quickly acquire coatings and become internally mixed (Gong  
476 et al., 2016; McMeeking et al., 2011; Moteki et al., 2007). Consequently, externally mixed BC  
477 particles are likely rare in the remote atmosphere. However, there is still little information about

478 the aerosol mixing state in aged air masses, especially at high latitudes (Raatikainen et al., 2015).  
479 In the baseline OsloCTM2-M7, a considerable fraction of total BC is in the insoluble Aitken  
480 mode BC (BCi) (45%, or 60 Gg, of the global BC burden with an aging time scale of 2.7 days).  
481 In particular, BCi constitutes the dominating fraction of total annual mean BC concentration  
482 north and south of 60° (Fig. SI4 b). However, there are important seasonal variations and high-  
483 latitude BCi concentration is highest during winter, when the aging is slower due to less  
484 efficient production of sulfate. Convective scavenging can be an important loss mechanism  
485 during Arctic winter, resulting in a considerable reduction in BC concentrations in the ConvBCi  
486 experiment. BCi also dominates above 300 hPa around the tropics.

487 The largest changes in concentration results from inclusion of condensation of nitric acid (Fig.  
488 3 i, Fig. S4 i). The number of MLs assumed as the criterion for aging is a key parameter.  
489 Different values have been assumed in studies with different aerosol schemes. Here we test the  
490 range of results under varying MLs in the same model. The resulting global burden and lifetime  
491 is approximately 40% higher in the simulation assuming 10 MLs than with 1 ML. The largest  
492 differences are found over South and East Asia (Fig. S5). With no firm agreement on the most  
493 correct number to use, we focus on results from the simulation with the middle value of 5 MLs  
494 in the following paragraphs.

495 Next, we examine the impact of the changes in concentrations on the existing model-  
496 measurement discrepancies. We focus on the Arctic stations (Alert, Barrow, Pallas and  
497 Zeppelin), as well as the vertical profiles from the aircraft campaigns discussed in Sect. 3.1.2.  
498 Figure 4 shows seasonal Arctic surface concentrations compared to the measurements (left  
499 column) and the absolute difference from the base in each experiment (right column). Figure 5  
500 shows the vertical BC profiles for each campaign and experiment, compared to the baseline and  
501 measurements.

502 **FIGURE 4**

503 **FIGURE 5**

504 A shorter atmospheric BC lifetime reduces the high-altitude overestimation at mid- and tropical  
505 latitudes over the Pacific. This is in line with other recent studies showing that modeled BC  
506 vertical profiles agree better with HIPPO data, in particular at higher altitudes, when the, which  
507 have suggested that the global BC lifetime is of BC in global models must be reduced in order  
508 for the models to reproduce the HIPPO data (Hodnebrog et al., 2014; Samset et al., 2014; Wang

509 et al., 2014). The MNB for the HIPPO campaigns is substantially reduced in the ConvBCi and  
510 CoatThick0.5 experiments compared to the baseline (from approx. 3 to -0.3 and 1, respectively).  
511 In most latitude bands, the reduction in MNB is largest for the former of the two. Given that  
512 the largest concentration changes in most of the experiments in the present analysis are found  
513 over the equatorial Atlantic (Fig. S4), a future comparison of our results against vertical profiles  
514 from the ongoing ATom campaign ([espo.nasa.gov/home/atom/content/ATom](https://espo.nasa.gov/home/atom/content/ATom)) will be a useful  
515 exercise. Our results are supported by Kipling et al. (2016), who also found convective  
516 scavenging to be an important parameter for the global vertical BC profile in the HadGEM3-  
517 UKCA. Surface concentrations at Alert, Zeppelin, and Pallas are also reproduced reasonably  
518 well in these experiments, although the springtime underestimation discussed above remains.  
519 In other parts of the Arctic however, the model performance is exacerbated. More specifically,  
520 the MNB for the ARCTAS and ARCPAC campaigns increases, and the underestimation of  
521 surface concentration at Barrow is larger compared to the baseline. Similar effects are also  
522 found in the 60°-70°S region (Fig. 5 e,j). Several other factors not considered here could also  
523 contribute to the too low modeled Arctic concentrations, including uncertainties in emissions  
524 and model resolution. For instance, a recently published study point to the importance of model  
525 resolution as a source of uncertainty, suggesting that a kilometer-order resolution is required  
526 for more accurate representation of BC concentrations in the Arctic (Sato et al., 2016).

527

528 Conversely, increasing the amount of soluble material required for aging increases the BC  
529 lifetime. This in turn results in an increased potential for long-range transport and increase in  
530 Arctic surface concentrations. However, with the exception of Barrow during spring, increasing  
531 the number of required ML (CoatThick1.4, CoatThick2.3) does not result in marked  
532 improvements in modeled Arctic surface concentrations compared to measurements. The  
533 modeled seasonal cycle in Arctic concentrations changes very little in all experiments. The  
534 longer aging time in CoatThick1.4 and CoatThick2.3 also results in a poorer agreement with  
535 the HIPPO measurements, both close to the surface and at high altitudes. Moreover, even with  
536 the longer lifetime and consequent increases in Arctic BC concentrations, the model does not  
537 reproduce the vertical profiles from ARCTAS and ARCPAC. These experiments also result in  
538 reduced concentrations of BC in snow in our model, since more BC resides in the insoluble  
539 mode, unavailable for wet scavenging. Hence, in the OsloCTM2-M7 a slower BC aging alone  
540 does not significant improve any model-measurement discrepancies.

541

542 Reducing the scavenging of BC by large-scale ice clouds and increasing the fraction of biomass  
543 burning emissions initially in the accumulation mode, have only a minor influence on the  
544 comparison with both Arctic surface concentrations and HIPPO profiles. The smaller impact in  
545 the former experiment contrasts the results by Fan et al. (2012), who found a good agreement  
546 with HIPPO data when reducing the removal efficiency of hydrophilic BC by snow in the AM3  
547 model. However, Fan et al. (2012) used a more detailed treatment of large-scale ice  
548 precipitation and adopted even lower scavenging coefficients than in our analysis.

549

550 Measurements at mid-latitudes have shown that nitrate is frequently present in internal aerosol  
551 mixtures and contribute to the aging of BC (Pratt & Prather, 2010; Shiraiwa et al., 2007). The  
552 addition of BC aging by nitric acid is a new development in the OsloCTM2-M7 and results  
553 from this experiment are discussed separately here. Allowing for nitric acid to condense on the  
554 aerosols results in a faster aging as more soluble material is available and hence reduces the  
555 global BC lifetime. This in turn reduces high-altitude BC concentrations and the discrepancies  
556 in the HIPPO comparison (MNB 0.4 and 0.7 for HIPPO1 and HIPPO2, respectively).  
557 Furthermore, BC snow concentrations across all regions except Greenland increase in this  
558 experiment, although not enough to fully account for the existing underestimation compared to  
559 measurements. However, the Arctic atmospheric BC concentrations are reduced, resulting in a  
560 poorer model performance compared to both measured vertical profiles and surface  
561 concentrations in this region. The work in this study is a first step and tests the potential  
562 importance of accounting for nitrate in the aerosol microphysics parameterization. There are,  
563 however, important limitations. For instance, the current setup only treats the condensation by  
564 nitric acid, not coagulation with nitrate aerosols. Another important caveat is that we do not  
565 account for changes in hydrophilicity resulting from evaporation of nitric acid already  
566 condensed on the aerosols. This may result in an overestimation of the contribution from nitric  
567 acid to the aging, at least in certain regions. In addition to nitrate, condensation of organic  
568 aerosols could play an important role in the aging of BC. For instance, He et al. (2016) recently  
569 found that a microphysics-based BC aging scheme including condensation of both nitric acid  
570 and secondary organics resulted in improved representation of BC in GEOS-Chem compared  
571 with HIPPO measurements. This process is currently not included in the OsloCTM2-M7, but  
572 should be addressed in future work.

573

574 Our analysis does not consider combinations of or regionally differing sensitivity experiments,  
575 for instance increased coating thickness required at high-latitudes in combination with more

576 efficient removal by convective precipitation in low and mid-latitudes. Moreover, there are  
577 important details that are not captured in the OsloCTM2-M7. One example is related to the  
578 particle hydrophilicity/hygroscopicity. The OsloCTM2-M7 assumes that particles can  
579 automatically act as cloud condensation nuclei once they are transferred from the hydrophobic  
580 to hydrophilic mode. However, the cloud condensating activity of hydrophilic and hygroscopic  
581 particles also depends on the atmospheric supersaturation (Koehler et al., 2009; Petters &  
582 Kreidenweis, 2007). Furthermore, particles may not merely be hydrophilic or not, as assumed  
583 by models, but can exhibit degrees of hydrophilicity. Our results underline the importance of  
584 more observations, in particular of the mixing state and scavenging of BC, as well as  
585 experimental data, to improve process understanding.

586

### 587 3.3 Climate impacts

588 As input to the discussion around the role of BC as a climate forcer, the impact of the changes  
589 in model parameters on radiative forcing (RF) and surface temperature (TS) is estimated using  
590 the kernel-based approach described in Sect. 2.4.

591 Figure 6 shows the change in BC ERFari (i.e., net of direct and semi-direct aerosol-radiation  
592 interactions), RFari (i.e., direct aerosol effect only) and TS in each experiment. Relative to the  
593 baseline, decreases in global-mean BC RFari up to  $-180 \text{ mW m}^{-2}$  are estimated for the two  
594 experiments that lead to the most marked improvements (i.e., strongest reduction in MNB) in  
595 vertical profiles compared to measurements over the Pacific (ConvBCi and NitCond) (Fig. 6).

596 A notable decrease in RFari of  $-90 \text{ mW m}^{-2}$  is also estimated for the CoatThick0.5 experiment.

597 These changes are on the order of 25-50% of the -RFari in the baseline simulation, estimated to  
598 be  $0.35 \text{ W m}^{-2}$ . The Fifth IPCC Assessment Report reports a best estimate of RFari (relative to  
599 pre-industrial) due to BC from all sources of  $0.6 \text{ W m}^{-2}$  (Boucher et al., 2013), while Bond et  
600 al. (2013) give a slightly higher estimate of  $0.71 \text{ W m}^{-2}$ . Hence, the changes in our  
601 sensitivity depending on experiments, the changes in global mean RFari estimated here are up  
602 on the order of 10 to 30% of the total best estimate BC RFari relative to pre-industrial. We  
603 emphasize that the RFari from the baseline simulation in the present study should not be  
604 compared with estimates of pre-industrial to present forcing by BC as it does not include the  
605 absorption enhancement due to BC aging and is given relative to a no-BC situation.

606 Including the semi-direct aerosol impacts partly offsets the RFari. The decrease in global-mean  
607 BC ERFari is  $-49$ ,  $-45$  and  $-26 \text{ mW m}^{-2}$  in the ConvBCi, NitCond and CoatThick0.5 experiments.

608 Changes in ERFari of similar magnitudes but opposite sign are estimated for the CoatThick1.4  
609 and CoatThick2.3 experiments. The change in TS is also largest for three former experiments,  
610 resulting in a decrease of -14 to -25 mK compared to the baseline (13-22% of the TS in the  
611 baseline simulation estimated using the kernel-based approach).

612 Both forcing and temperature response is sensitive to the altitude of BC concentration change.  
613 Figure 7 examines the vertical variability behind results in Fig. 6. The globally averaged ERFari  
614 (Fig. 7b) peaks below 900 hPa and around 200 hPa, driven by contributions from both the semi-  
615 direct and direct radiative effects. The direct radiative effect per BC burden increases with  
616 altitude (see also Fig.1 of Samset and Myhre (2015)), resulting in a larger change in RFar  
617 higher altitudes in the present analysis, especially in the ConvBCi and NitCond experiments  
618 (Fig. 7a). In contrast, the semi-direct effect per BC burden is positive below 900hPa, but  
619 negative and increasing in strength at higher altitudes. Between 800 and 400 hPa the ERFari is  
620 smaller due to cancelling direct and semi-direct effects. The net changes in ERFari in Fig.6 are  
621 thus largely determined by an RFar contribution due high altitude concentration changes in our  
622 experiments and a low altitude contribution from the semi-direct effect. The TS change is  
623 largest in the lower models layers (Fig. 7c), in agreement with the decreasing efficacy of BC  
624 forcing with altitude.

625 We also estimate the changes in Arctic ERFari and TS (not shown here). These are generally  
626 larger than the global mean changes. In the CoatThick and NitCond experiments, we estimate  
627 30-50% higher change in ERFari due to Arctic BC concentration changes compared to the  
628 global mean change. This reflects that the concentration changes are larger in the lower model  
629 layers at high northern latitudes in these experiments (Fig. 3), combined with a stronger direct  
630 radiative efficiency over this region and a relatively smaller semi-direct effect, which offsets  
631 less of the RFar than globally averaged. Surface temperature response per BC burden is also  
632 larger for low altitude perturbations at high latitudes than globally averaged, and even becomes  
633 slightly negative, i.e., a cooling, above 400 hPa north of 70°N. The low altitude concentration  
634 changes in Arctic therefore also results in larger TS changes (by a factor 2-4) compared to the  
635 global mean change.

636 There is, however, an important caveat when using the temperature kernel from Samset and  
637 Myhre (2015) to estimate Arctic changes. Because globally uniform BC perturbations were  
638 imposed in each model layer, the impact on temperature in a specific gridbox may be due both  
639 to forcing exerted locally and to remote forcing through large-scale circulation impacts. To

640 exclude any possible influence of BC forcing exerted outside the Arctic region, we also use  
641 results from Flanner (2013) to estimate the change in Arctic TS. Flanner (2013) imposed BC  
642 perturbations at five different altitudes over the Arctic only, using the same model as Samset  
643 and Myhre (2015), hence calculating the Arctic TS caused only by a local perturbation. The  
644 resulting temperature kernel has previously been used to assess the impact of regional on-road  
645 diesel BC emissions (Lund et al., 2014). When used here to estimate the impact of our  
646 experiments, we find similar changes in Arctic TS to those estimated using results from Samset  
647 and Myhre (2015), with some small differences. In the LSice12 and CombPert experiments, the  
648 changes in net Arctic TS estimated using Flanner (2013) are of opposite sign from results using  
649 the kernel from Samset and Myhre (2015). This is caused by different efficacies above 500 hPa,  
650 where these experiments give the largest changes in Arctic BC concentrations.

651

#### 652 **4 Summary and conclusions**

653 We have performed a range of experiments to investigate the sensitivity of BC concentrations  
654 modeled by the OsloCTM2-M7 to parameters controlling the aerosol scavenging and aging,  
655 including, for the first time in the model, a treatment of condensation of nitric acid on BC  
656 particles. The impact of changes in these processes on the existing model-measurement  
657 discrepancies in Arctic surface concentrations and high-altitude concentrations over remote  
658 regions of the Pacific is investigated, in order to identify potential improvements to be included  
659 in future work. Our analysis is further extended to include an assessment of the effect of the  
660 concentration changes on subsequent radiative forcing and surface temperature response.

661

662 We find changes of up to 40% in global BC burden and lifetime compared to the baseline, with  
663 the largest decreases resulting from inclusion of convective scavenging of hydrophobic BC and  
664 aging by nitric acid condensation. In most experiments, the largest changes in concentrations  
665 are found in lower model layers north of 60°N and at higher altitudes around the equatorial  
666 Atlantic. In the experiments resulting the most pronounced BC concentration changes relative  
667 to the baseline, we calculate changes in global-mean RF<sub>ari</sub> (i.e., direct RF) on the order of 10-  
668 30% of the total pre-industrial to present BC direct forcing. However, even with the  
669 considerable changes in concentrations, the total impact (i.e., net of direct and semi-direct  
670 aerosol-radiation interactions) on global mean surface temperature is estimated to less than  
671 0.04K.

672 A shorter atmospheric BC lifetime in the OsloCTM2-M7 reduces the high-altitude  
673 overestimation at mid- and tropical latitudes over the Pacific and improves the comparison with  
674 HIPPO measurement data, providing further support to findings from recent studies  
675 (Hodnebrog et al., 2014; Samset et al., 2014; Wang et al., 2014). However, this required shorter  
676 lifetime can be achieved through changes in several different model parameters. Both inclusion  
677 of convective scavenging of hydrophobic BC and reduction in the amount of soluble material  
678 required for BC aging results in a 60 to 90 percent lower MNB in the comparison with vertical  
679 profiles from HIPPO, relative to the baseline. In the case of convective scavenging, the model  
680 is sensitive to the fraction of hydrophobic BC assumed to be available for removal, which is a  
681 poorly constrained parameter. The OsloCTM2-M7 is better able to reproduce the observed  
682 seasonal variation and magnitude of Arctic BC surface concentrations compared to previous  
683 OsloCTM2 studies, although model-measurement discrepancies remain, particularly during  
684 spring. Surface concentrations at Alert, Zeppelin and Pallas remain in reasonable agreement  
685 with observations in the two abovementioned experiments, but the agreement with  
686 measurements at Barrow becomes poorer.

687 We also find similar improvements in the comparison with HIPPO measurements when  
688 including BC aging by condensation of nitric acid. However, the Arctic atmospheric BC  
689 concentrations are substantially reduced, resulting in a poorer model performance compared to  
690 both measured vertical profiles and surface concentrations in the region. The treatment of BC  
691 aging by nitric acid included here is a first step. Further work to resolve uncertainties and  
692 incorporate missing processes, such as coagulation with nitrate aerosols and secondary organics,  
693 is needed for the development of a more comprehensive aerosol microphysical parameterization  
694 in the OsloCTM2-M7.

695  
696 The existing model-measurement discrepancies in the OsloCTM2-M7 can not be uniquely  
697 attributed to uncertainties in a single process or parameter. Furthermore, improvements  
698 compared to measurements in one geographical region, can be accompanied by a poorer model  
699 performance in other. This underlines the need for better process understanding supported by  
700 observational and experimental data, e.g., of BC IN efficiency, aging rate and mixing state,  
701 rather than tuning of individual, effective parameters such as global BC lifetime, to further  
702 improve models and constrain estimates of BC climate impact. Sensitivity studies may therefore  
703 provide important insight ahead of upcoming measurement campaigns regarding where

704 experimental efforts could be focused in order to provide the best possible data for further  
705 constraining global models.

706

707

708

### 709 **Acknowledgements**

710 This work was funded by the Research Council of Norway through the projects TEMPO,  
711 SLAC, AC/BC and QUISARC. We also acknowledge the Reseach Council of Norway's  
712 programme for supercomputing (NOTUR). We thank Professor Yutaka Kondo, University of  
713 Tokyo, for providing results from the A-FORCE flight campaign.

714

715

716

717

718

719

720

721

722

723

724

725

726

727

728

729

730 **References:**

- 731 Allen R. J. & Landuyt W. (2014). The vertical distribution of black carbon in CMIP5 models:  
732 Comparison to observations and the importance of convective transport. *Journal of Geophysical*  
733 *Research: Atmospheres*. 119(8), 4808-4835, DOI: 10.1002/2014JD021595.
- 734 AMAP (2015). AMAP Assessment 2015: Black carbon and ozone as Arctic climate forcers.  
735 Arctic Monitoring and Assessment Programme (AMAP), Oslo, Norway.
- 736 Anenberg S. C., Schwartz J., Shindell D., Amann M., Faluvegi G., Klimont Z., Janssens-  
737 Maenhout G., Pozzoli L., Van Dingenen R., Vignati E., Emberson L., Muller N. Z., West J. J., Williams  
738 M., Demkine V., Hicks W. K., Kuylensstierna J., Raes F. & Ramanathan V. (2012). Global Air Quality and  
739 Health Co-benefits of Mitigating Near-Term Climate Change through Methane and Black Carbon  
740 Emission Controls. *Environmental Health Perspectives*. 120(6), 831-839, DOI: 10.1289/ehp.1104301.
- 741 Aunan K., Fang J., Hu T., Seip H. M. & Vennemo H. (2006). Climate Change and Air Quality—  
742 Measures with Co-Benefits in China. *Environmental Science & Technology*. 40(16), 4822-4829, DOI:  
743 10.1021/es062994k.
- 744 Balkanski Y., Myhre G., Gauss M., Raedel G., Highwood E. J. & Shine K. P. (2010). Direct  
745 radiative effect of aerosols emitted by transport: from road, shipping and aviation. *Atmospheric*  
746 *Chemistry and Physics*. 10(10), 4477-4489, DOI: 10.5194/acp-10-4477-2010.
- 747 Ban-Weiss G., Cao L., Bala G. & Caldeira K. (2011). Dependence of climate forcing and  
748 response on the altitude of black carbon aerosols. *Climate Dynamics*, 1-15, DOI: 10.1007/s00382-  
749 011-1052-y.
- 750 Bauer S. E., Koch D., Unger N., Metzger S. M., Shindell D. T. & Streets D. G. (2007). Nitrate  
751 aerosols today and in 2030: a global simulation including aerosols and tropospheric ozone.  
752 *Atmospheric Chemistry and Physics*. 7(19), 5043-5059.
- 753 Bellouin N., Rae J., Jones A., Johnson C., Haywood J. & Boucher O. (2011). Aerosol forcing in  
754 the Climate Model Intercomparison Project (CMIP5) simulations by HadGEM2-ES and the role of  
755 ammonium nitrate. *Journal of Geophysical Research-Atmospheres*. 116, D20206, DOI:  
756 10.1029/2011jd016074.
- 757 Berge E. (1993). Coupling of wet scavenging of sulphur to clouds in a numerical weather  
758 prediction model. *Tellus B*. 45(1), 1-22, DOI: 10.1034/j.1600-0889.1993.00001.x.
- 759 Berglen T. F., Berntsen T. K., Isaksen I. S. A. & Sundet J. K. (2004). A global model of the  
760 coupled sulfur/oxidant chemistry in the troposphere: The sulfur cycle. *Journal of Geophysical*  
761 *Research-Atmospheres*. 109(D19), D19310, DOI: 10.1029/2003jd003948.
- 762 Berntsen T., Fuglestad J., Myhre G., Stordal F. & Berglen T. F. (2006). Abatement of  
763 greenhouse gases: Does location matter? *Climatic Change*. 74(4), 377-411, DOI: 10.1007/s10584-  
764 006-0433-4.
- 765 Berntsen T. K. & Isaksen I. S. A. (1997). A global three-dimensional chemical transport model  
766 for the troposphere .1. Model description and CO and ozone results. *Journal of Geophysical*  
767 *Research-Atmospheres*. 102(D17), 21239-21280, DOI: 10.1029/97jd01140.
- 768 Bollasina M. A., Ming Y., Ramaswamy V., Schwarzkopf M. D. & Naik V. (2014). Contribution  
769 of local and remote anthropogenic aerosols to the twentieth century weakening of the South Asian  
770 Monsoon. *Geophysical Research Letters*. 41(2), 680-687, DOI: 10.1002/2013GL058183.
- 771 Bond T. C. & Bergstrom R. W. (2006). Light absorption by carbonaceous particles: An  
772 investigative review. *Aerosol Science and Technology*. 40(1), 27-67, DOI:  
773 10.1080/02786820500421521.
- 774 Bond T. C., Doherty S. J., Fahey D. W., Forster P. M., Berntsen T., DeAngelo B. J., Flanner M.  
775 G., Ghan S., Kärcher B., Koch D., Kinne S., Kondo Y., Quinn P. K., Sarofim M. C., Schultz M. G., Schulz  
776 M., Venkataraman C., Zhang H., Zhang S., Bellouin N., Guttikunda S. K., Hopke P. K., Jacobson M. Z.,  
777 Kaiser J. W., Klimont Z., Lohmann U., Schwarz J. P., Shindell D., Storelvmo T., Warren S. G. & Zender  
778 C. S. (2013). Bounding the role of black carbon in the climate system: A scientific assessment.  
779 *Journal of Geophysical Research: Atmospheres*. 118(11), 5380-5552, DOI: 10.1002/jgrd.50171.

780 Boucher O., Randall D., Artaxo P., Bretherton C., Feingold G., Forster P., Kerminen V.-M.,  
781 Kondo Y., Liao H., Lohmann U., Rasch P., Satheesh S. K., Sherwood S., Stevens B. & Zhang X. Y.  
782 (2013). Clouds and Aerosols. In: Climate Change 2013: The Physical Science Basis. Contribution of  
783 Working Group I to the Fifth Assessment Report of the Intergovernmental Panel on Climate Change  
784 [Stocker, T.F., D. Qin, G.-K. Plattner, M. Tignor, S.K. Allen, J. Boschung, A. Nauels, Y. Xia, V. Bex and  
785 P.M. Midgley (eds.)]. Cambridge University Press, Cambridge, United Kingdom and New York, NY,  
786 USA.

787 Bourgeois Q. & Bey I. (2011). Pollution transport efficiency toward the Arctic: Sensitivity to  
788 aerosol scavenging and source regions. *Journal of Geophysical Research: Atmospheres*. 116(D8), n/a-  
789 n/a, DOI: 10.1029/2010JD015096.

790 Bouwman A. F., Lee D. S., Asman W. A. H., Dentener F. J., Van Der Hoek K. W. & Olivier J. G. J.  
791 (1997). A global high-resolution emission inventory for ammonia. *Global Biogeochemical Cycles*.  
792 11(4), 561-587, DOI: 10.1029/97GB02266.

793 Bowerman N. H. A., Frame D. J., Huntingford C., Lowe J. A., Smith S. M. & Allen M. R. (2013).  
794 The role of short-lived climate pollutants in meeting temperature goals. *Nature Clim. Change*. 3(12),  
795 1021-1024, DOI: 10.1038/nclimate2034.

796 Breider T. J., Mickley L. J., Jacob D. J., Wang Q., Fisher J. A., Chang R. Y. W. & Alexander B.  
797 (2014). Annual distributions and sources of Arctic aerosol components, aerosol optical depth, and  
798 aerosol absorption. *Journal of Geophysical Research: Atmospheres*. 119(7), 4107-4124, DOI:  
799 10.1002/2013JD020996.

800 Brock C. A., Cozic J., Bahreini R., Froyd K. D., Middlebrook A. M., McComiskey A., Brioude J.,  
801 Cooper O. R., Stohl A., Aikin K. C., de Gouw J. A., Fahey D. W., Ferrare R. A., Gao R. S., Gore W.,  
802 Holloway J. S., Hübler G., Jefferson A., Lack D. A., Lance S., Moore R. H., Murphy D. M., Nenes A.,  
803 Novelli P. C., Nowak J. B., Ogren J. A., Peischl J., Pierce R. B., Pilewskie P., Quinn P. K., Ryerson T. B.,  
804 Schmidt K. S., Schwarz J. P., Sodemann H., Spackman J. R., Stark H., Thomson D. S., Thornberry T.,  
805 Veres P., Watts L. A., Warneke C. & Wollny A. G. (2011). Characteristics, sources, and transport of  
806 aerosols measured in spring 2008 during the aerosol, radiation, and cloud processes affecting Arctic  
807 Climate (ARCPAC) Project. *Atmos. Chem. Phys.* 11(6), 2423-2453, DOI: 10.5194/acp-11-2423-2011.

808 Browse J., Carslaw K. S., Arnold S. R., Pringle K. & Boucher O. (2012). The scavenging  
809 processes controlling the seasonal cycle in Arctic sulphate and black carbon aerosol. *Atmospheric  
810 Chemistry and Physics*. 12(15), 6775-6798, DOI: 10.5194/acp-12-6775-2012.

811 Cozic J., Verheggen B., Mertes S., Connolly P., Bower K., Petzold A., Baltensperger U. &  
812 Weingartner E. (2007). Scavenging of black carbon in mixed phase clouds at the high alpine site  
813 Jungfraujoch. *Atmospheric Chemistry and Physics*. 7(7), 1797-1807.

814 Doherty S. J., Warren S. G., Grenfell T. C., Clarke A. D. & Brandt R. E. (2010). Light-absorbing  
815 impurities in Arctic snow. *Atmospheric Chemistry and Physics*. 10, 11647-11680.

816 Eckhardt S., Quennehen B., Olivie D. J. L., Berntsen T. K., Cherian R., Christensen J. H., Collins  
817 W., Crepinsek S., Daskalakis N., Flanner M., Herber A., Heyes C., Hodnebrog Ø., Huang L., Kanakidou  
818 M., Klimont Z., Langner J., Law K. S., Lund M. T., Mahmood R., Massling A., Myriokefalitakis S.,  
819 Nielsen I. E., Nøjgaard J. K., Quaas J., Quinn P. K., Raut J. C., Rumbold S. T., Schulz M., Sharma S., Skeie  
820 R. B., Skov H., Uttal T., von Salzen K. & Stohl A. (2015). Current model capabilities for simulating  
821 black carbon and sulfate concentrations in the Arctic atmosphere: a multi-model evaluation using a  
822 comprehensive measurement data set. *Atmos. Chem. Phys.* 15(16), 9413-9433, DOI: 10.5194/acp-  
823 15-9413-2015.

824 Ekman A. M. L., Wang C., Strom J. & Krejci R. (2006). Explicit simulation of aerosol physics in  
825 a cloud-resolving model: Aerosol transport and processing in the free troposphere. *J. Atmos. Sci.*  
826 63(2), 682-696, DOI: 10.1175/jas3645.1.

827 Emmons L. K., Arnold S. R., Monks S. A., Huijnen V., Tilmes S., Law K. S., Thomas J. L., Raut J.  
828 C., Bouarar I., Turquety S., Long Y., Duncan B., Steenrod S., Strode S., Flemming J., Mao J., Langner J.,  
829 Thompson A. M., Tarasick D., Apel E. C., Blake D. R., Cohen R. C., Dibb J., Diskin G. S., Fried A., Hall S.  
830 R., Huey L. G., Weinheimer A. J., Wisthaler A., Mikoviny T., Nowak J., Peischl J., Roberts J. M., Ryerson  
831 T., Warneke C. & Helmig D. (2015). The POLARCAT Model Intercomparison Project (POLMIP):

832 overview and evaluation with observations. *Atmos. Chem. Phys.* 15(12), 6721-6744, DOI:  
833 10.5194/acp-15-6721-2015.

834 EPA (2012). Report to Congress on black carbon. US Environmental Protection Agency,  
835 Washington DC, USA.

836 Fan S. M., Schwarz J. P., Liu J., Fahey D. W., Ginoux P., Horowitz L. W., Levy H., Ming Y. &  
837 Spackman J. R. (2012). Inferring ice formation processes from global-scale black carbon profiles  
838 observed in the remote atmosphere and model simulations. *Journal of Geophysical Research:*  
839 *Atmospheres.* 117(D23), n/a-n/a, DOI: 10.1029/2012JD018126.

840 Flanner M. G., Zender C. S., Hess P. G., Mahowald N. M., Painter T. H., Ramanathan V. &  
841 Rasch P. J. (2009). Springtime warming and reduced snow cover from carbonaceous particles.  
842 *Atmospheric Chemistry and Physics.* 9(7), 2481-2497.

843 Flanner M. G. (2013). Arctic climate sensitivity to local black carbon. *Journal of Geophysical*  
844 *Research-Atmospheres.* 118(4), 1840-1851, DOI: 10.1002/jgrd.50176.

845 Fujino J., Nair R., Kainuma M., Masui T. & Matsuoka Y. (2006). Multi-gas mitigation analysis  
846 on stabilization scenarios using AIM global model. *Energy Journal.* Special issue: 3, 343-353.

847 Gong X., Zhang C., Chen H., Nizkorodov S. A., Chen J. & Yang X. (2016). Size distribution and  
848 mixing state of black carbon particles during a heavy air pollution episode in Shanghai. *Atmos. Chem.*  
849 *Phys.* 16(8), 5399-5411, DOI: 10.5194/acp-16-5399-2016.

850 Grieshop A. P., Reynolds C. C. O., Kandlikar M. & Dowlatabadi H. (2009). A black-carbon  
851 mitigation wedge. *Nature Geoscience.* 2(8), 533-534, DOI: 10.1038/ngeo595.

852 Guenther A. B., Jiang X., Heald C. L., Sakulyanontvittaya T., Duhl T., Emmons L. K. & Wang X.  
853 (2012). The Model of Emissions of Gases and Aerosols from Nature version 2.1 (MEGAN2.1): an  
854 extended and updated framework for modeling biogenic emissions. *Geosci. Model Dev.* 5(6), 1471-  
855 1492, DOI: 10.5194/gmd-5-1471-2012.

856 He C., Li Q., Liou K. N., Qi L., Tao S. & Schwarz J. P. (2016). Microphysics-based black carbon  
857 aging in a global CTM: constraints from HIPPO observations and implications for global black carbon  
858 budget. *Atmos. Chem. Phys.* 16(5), 3077-3098, DOI: 10.5194/acp-16-3077-2016.

859 Hijioka J., Matsuoka Y., Nishimoto H., Masui M. & Kainuma M. (2008). Global GHG emissions  
860 scenarios under GHG concentration stabilization targets. *Journal of Global Environmental*  
861 *Engineering.* 13, 97-108.

862 Hodnebrog Ø., Myhre G. & Samset B. H. (2014). How shorter black carbon lifetime alters its  
863 climate effect. *Nat Commun.* 5, DOI: 10.1038/ncomms6065.

864 Hoose C., Kristjansson J. E., Chen J. P. & Hazra A. (2010). A Classical-Theory-Based  
865 Parameterization of Heterogeneous Ice Nucleation by Mineral Dust, Soot, and Biological Particles in a  
866 Global Climate Model. *J. Atmos. Sci.* 67(8), 2483-2503, DOI: 10.1175/2010jas3425.1.

867 Huang K., Fu J. S., Prikhodko V. Y., Storey J. M., Romanov A., Hodson E. L., Cresko J.,  
868 Morozova I., Ignatieva Y. & Cabaniss J. (2015). Russian anthropogenic black carbon: Emission  
869 reconstruction and Arctic black carbon simulation. *Journal of Geophysical Research: Atmospheres.*  
870 120(21), 11,306-311,333, DOI: 10.1002/2015JD023358.

871 Jacob D. J., Crawford J. H., Maring H., Clarke A. D., Dibb J. E., Emmons L. K., Ferrare R. A.,  
872 Hostetler C. A., Russell P. B., Singh H. B., Thompson A. M., Shaw G. E., McCauley E., Pederson J. R. &  
873 Fisher J. A. (2010). The Arctic Research of the Composition of the Troposphere from Aircraft and  
874 Satellites (ARCTAS) mission: design, execution, and first results. *Atmos. Chem. Phys.* 10(11), 5191-  
875 5212, DOI: 10.5194/acp-10-5191-2010.

876 Kajino M., Inomata Y., Sato K., Ueda H., Han Z., An J., Katata G., Deushi M., Maki T., Oshima  
877 N., Kurokawa J., Ohara T., Takami A. & Hatakeyama S. (2012). Development of the RAQM2 aerosol  
878 chemical transport model and predictions of the Northeast Asian aerosol mass, size, chemistry, and  
879 mixing type. *Atmospheric Chemistry and Physics.* 12(24), 11833-11856, DOI: 10.5194/acp-12-11833-  
880 2012.

881 Kipling Z., Stier P., Schwarz J. P., Perring A. E., Spackman J. R., Mann G. W., Johnson C. E. &  
882 Telford P. J. (2013). Constraints on aerosol processes in climate models from vertically-resolved

883 aircraft observations of black carbon. *Atmos. Chem. Phys.* 13(12), 5969-5986, DOI: 10.5194/acp-13-  
884 5969-2013.

885 Kipling Z., Stier P., Johnson C. E., Mann G. W., Bellouin N., Bauer S. E., Bergman T., Chin M.,  
886 Diehl T., Ghan S. J., Iversen T., Kirkevåg A., Kokkola H., Liu X., Luo G., van Noije T., Pringle K. J.,  
887 von Salzen K., Schulz M., Seland Ø., Skeie R. B., Takemura T., Tsigaridis K. & Zhang K. (2016). What  
888 controls the vertical distribution of aerosol? Relationships between process sensitivity in HadGEM3–  
889 UKCA and inter-model variation from AeroCom Phase II. *Atmos. Chem. Phys.* 16(4), 2221-2241, DOI:  
890 10.5194/acp-16-2221-2016.

891 Klimont Z., Kupiainen K., Heyes C., Purohit P., Cofala J., Rafaj P., Borcken-Kleefeld J. & Schöpp  
892 W. (2016). Global anthropogenic emissions of particulate matter including black carbon. *Atmos.*  
893 *Chem. Phys. Discuss.* 2016, 1-72, DOI: 10.5194/acp-2016-880.

894 Koch D., Menon S., Del Genio A., Ruedy R., Alienov I. & Schmidt G. A. (2009a). Distinguishing  
895 Aerosol Impacts on Climate over the Past Century. *Journal of Climate.* 22(10), 2659-2677, DOI:  
896 10.1175/2008jcli2573.1.

897 Koch D., Schulz M., Kinne S., McNaughton C., Spackman J. R., Balkanski Y., Bauer S., Berntsen  
898 T., Bond T. C., Boucher O., Chin M., Clarke A., De Luca N., Dentener F., Diehl T., Dubovik O., Easter R.,  
899 Fahey D. W., Feichter J., Fillmore D., Freitag S., Ghan S., Ginoux P., Gong S., Horowitz L., Iversen T.,  
900 Kirkevåg A., Klimont Z., Kondo Y., Krol M., Liu X., Miller R., Montanaro V., Moteki N., Myhre G.,  
901 Penner J. E., Perlwitz J., Pitari G., Reddy S., Sahu L., Sakamoto H., Schuster G., Schwarz J. P., Seland O.,  
902 Stier P., Takegawa N., Takemura T., Textor C., van Aardenne J. A. & Zhao Y. (2009b). Evaluation of  
903 black carbon estimations in global aerosol models. *Atmospheric Chemistry and Physics.* 9(22), 9001-  
904 9026, DOI: 10.5194/acp-9-9001-2009.

905 Koch D. & Del Genio A. D. (2010). Black carbon semi-direct effects on cloud cover: review  
906 and synthesis. *Atmospheric Chemistry and Physics.* 10(16), 7685-7696, DOI: 10.5194/acp-10-7685-  
907 2010.

908 Koehler K. A., DeMott P. J., Kreidenweis S. M., Popovicheva O. B., Petters M. D., Carrico C. M.,  
909 Kireeva E. D., Khokhlova T. D. & Shonija N. K. (2009). Cloud condensation nuclei and ice nucleation  
910 activity of hydrophobic and hydrophilic soot particles. *Physical Chemistry Chemical Physics.* 11(36),  
911 7906-7920, DOI: 10.1039/b905334b.

912 Kopp R. E. & Mauzerall D. L. (2010). Assessing the climatic benefits of black carbon  
913 mitigation. *Proceedings of the National Academy of Sciences of the United States of America.*  
914 107(26), 11703-11708, DOI: 10.1073/pnas.0909605107.

915 Lee Y. H., Lamarque J. F., Flanner M. G., Jiao C., Shindell D. T., Berntsen T., Bisiaux M. M., Cao  
916 J., Collins W. J., Curran M., Edwards R., Faluvegi G., Ghan S., Horowitz L. W., McConnell J. R., Ming J.,  
917 Myhre G., Nagashima T., Naik V., Rumbold S. T., Skeie R. B., Sudo K., Takemura T., Thevenon F., Xu B.  
918 & Yoon J. H. (2013). Evaluation of preindustrial to present-day black carbon and its albedo forcing  
919 from Atmospheric Chemistry and Climate Model Intercomparison Project (ACCMIP). *Atmospheric*  
920 *Chemistry and Physics.* 13(5), 2607-2634, DOI: 10.5194/acp-13-2607-2013.

921 Liu J., Fan S., Horowitz L. W. & Levy H., II (2011). Evaluation of factors controlling long-range  
922 transport of black carbon to the Arctic. *Journal of Geophysical Research-Atmospheres.* 116, D04307,  
923 DOI: 10.1029/2010jd015145.

924 Lohmann U. & Feichter J. (2005). Global indirect aerosol effects: a review. *Atmos. Chem.*  
925 *Phys.* 5(3), 715-737, DOI: 10.5194/acp-5-715-2005.

926 Lund M. T. & Berntsen T. (2012). Parameterization of black carbon aging in the OsloCTM2  
927 and implications for regional transport to the Arctic. *Atmos. Chem. Phys.* 12(15), 6999-7014, DOI:  
928 10.5194/acp-12-6999-2012.

929 Lund M. T., Berntsen T. K., Heyes C., Klimont Z. & Samset B. H. (2014). Global and regional  
930 climate impacts of black carbon and co-emitted species from the on-road diesel sector. *Atmospheric*  
931 *Environment.* 98, 50-58, DOI: <http://dx.doi.org/10.1016/j.atmosenv.2014.08.033>.

932 Mahmood R., von Salzen K., Flanner M., Sand M., Langner J., Wang H. & Huang L. (2016).  
933 Seasonality of global and Arctic black carbon processes in the Arctic Monitoring and Assessment

934 Programme models. *Journal of Geophysical Research: Atmospheres*. 121(12), 7100-7116, DOI:  
935 10.1002/2016JD024849.

936 Makkonen R., Romakkaniemi S., Kokkola H., Stier P., Raisanen P., Rast S., Feichter J., Kulmala  
937 M. & Laaksonen A. (2012). Brightening of the global cloud field by nitric acid and the associated  
938 radiative forcing. *Atmospheric Chemistry and Physics*. 12(16), 7625-7633, DOI: 10.5194/acp-12-7625-  
939 2012.

940 Mann G. W., Carslaw K. S., Spracklen D. V., Ridley D. A., Manktelow P. T., Chipperfield M. P.,  
941 Pickering S. J. & Johnson C. E. (2010). Description and evaluation of GLOMAP-mode: a modal global  
942 aerosol microphysics model for the UKCA composition-climate model. *Geosci. Model Dev.* 3(2), 519-  
943 551, DOI: 10.5194/gmd-3-519-2010.

944 McMeeking G. R., Morgan W. T., Flynn M., Highwood E. J., Turnbull K., Haywood J. & Coe H.  
945 (2011). Black carbon aerosol mixing state, organic aerosols and aerosol optical properties over the  
946 United Kingdom. *Atmospheric Chemistry and Physics*. 11(17), 9037-9052, DOI: 10.5194/acp-11-9037-  
947 2011.

948 Metzger S., Dentener F., Krol M., Jeuken A. & Lelieveld J. (2002a). Gas/aerosol partitioning -  
949 2. Global modeling results. *Journal of Geophysical Research-Atmospheres*. 107(D16), 4313, DOI:  
950 10.1029/2001jd001103.

951 Metzger S., Dentener F., Pandis S. & Lelieveld J. (2002b). Gas/aerosol partitioning: 1. A  
952 computationally efficient model. *Journal of Geophysical Research-Atmospheres*. 107(D16), 4312,  
953 DOI: 10.1029/2001jd001102.

954 Monks S. A., Arnold S. R., Emmons L. K., Law K. S., Turquety S., Duncan B. N., Flemming J.,  
955 Huijnen V., Tilmes S., Langner J., Mao J., Long Y., Thomas J. L., Steenrod S. D., Raut J. C., Wilson C.,  
956 Chipperfield M. P., Diskin G. S., Weinheimer A., Schlager H. & Ancellet G. (2015). Multi-model study  
957 of chemical and physical controls on transport of anthropogenic and biomass burning pollution to the  
958 Arctic. *Atmos. Chem. Phys.* 15(6), 3575-3603, DOI: 10.5194/acp-15-3575-2015.

959 Moteki N., Kondo Y., Miyazaki Y., Takegawa N., Komazaki Y., Kurata G., Shirai T., Blake D. R.,  
960 Miyakawa T. & Koike M. (2007). Evolution of mixing state of black carbon particles: Aircraft  
961 measurements over the western Pacific in March 2004. *Geophysical Research Letters*. 34(11),  
962 L11803, DOI: 10.1029/2006gl028943.

963 Myhre G., Grini A. & Metzger S. (2006). Modelling of nitrate and ammonium-containing  
964 aerosols in presence of sea salt. *Atmos. Chem. Phys.* 6, 4809-4821.

965 Myhre G., Samset B. H., Schulz M., Balkanski Y., Bauer S., Bernsten T. K., Bian H., Bellouin N.,  
966 Chin M., Diehl T., Easter R. C., Feichter J., Ghan S. J., Hauglustaine D., Iversen T., Kinne S., Kirkevåg A.,  
967 Lamarque J. F., Lin G., Liu X., Lund M. T., Luo G., Ma X., van Noije T., Penner J. E., Rasch P. J., Ruiz A.,  
968 Seland O., Skeie R. B., Stier P., Takemura T., Tsigaridis K., Wang P., Wang Z., Xu L., Yu H., Yu F., Yoon J.  
969 H., Zhang K., Zhang H. & Zhou C. (2013). Radiative forcing of the direct aerosol effect from AeroCom  
970 Phase II simulations. *Atmospheric Chemistry and Physics*. 13(4), 1853-1877, DOI: 10.5194/acp-13-  
971 1853-2013.

972 Oshima N., Kondo Y., Moteki N., Takegawa N., Koike M., Kita K., Matsui H., Kajino M.,  
973 Nakamura H., Jung J. S. & Kim Y. J. (2012). Wet removal of black carbon in Asian outflow: Aerosol  
974 Radiative Forcing in East Asia (A-FORCE) aircraft campaign. *Journal of Geophysical Research-  
975 Atmospheres*. 117, D03204, DOI: 10.1029/2011jd016552.

976 Park R. J., Jacob D. J., Palmer P. I., Clarke A. D., Weber R. J., Zondlo M. A., Eisele F. L., Bandy A.  
977 R., Thornton D. C., Sachse G. W. & Bond T. C. (2005). Export efficiency of black carbon aerosol in  
978 continental outflow: Global implications. *Journal of Geophysical Research-Atmospheres*. 110(D11),  
979 D11205, DOI: 10.1029/2004jd005432.

980 Petters M. D. & Kreidenweis S. M. (2007). A single parameter representation of hygroscopic  
981 growth and cloud condensation nucleus activity. *Atmospheric Chemistry and Physics*. 7(8), 1961-  
982 1971.

983 Petzold A., Ogren J. A., Fiebig M., Laj P., Li S. M., Baltensperger U., Holzer-Popp T., Kinne S.,  
984 Pappalardo G., Sugimoto N., Wehrli C., Wiedensohler A. & Zhang X. Y. (2013). Recommendations for

985 reporting "black carbon" measurements. *Atmos. Chem. Phys.* 13(16), 8365-8379, DOI: 10.5194/acp-  
986 13-8365-2013.

987 Popovicheva O. B., Persiantseva N. M., Tishkova V., Shonija N. K. & Zubareva N. A. (2008).  
988 Quantification of water uptake by soot particles. *Environmental Research Letters*. 3(2), 025009, DOI:  
989 10.1088/1748-9326/3/2/025009.

990 Popovicheva O. B., Persiantseva N. M., Kireeva E. D., Khokhlova T. D. & Shonija N. K. (2011).  
991 Quantification of the Hygroscopic Effect of Soot Aging in the Atmosphere: Laboratory Simulations.  
992 *Journal of Physical Chemistry A*. 115(3), 298-306, DOI: 10.1021/jp109238x.

993 Pratt K. A. & Prather K. A. (2010). Aircraft measurements of vertical profiles of aerosol mixing  
994 states. *Journal of Geophysical Research-Atmospheres*. 115, D11305, DOI: 10.1029/2009jd013150.

995 Pringle K. J., Tost H., Message S., Steil B., Giannadaki D., Nenes A., Fountoukis C., Stier P.,  
996 Vignati E. & Lelieveld J. (2010). Description and evaluation of GMXe: a new aerosol submodel for  
997 global simulations (v1). *Geoscientific Model Development*. 3(2), 391-412, DOI: 10.5194/gmd-3-391-  
998 2010.

999 Raatikainen T., Brus D., Hyvärinen A. P., Svensson J., Asmi E. & Lihavainen H. (2015). Black  
1000 carbon concentrations and mixing state in the Finnish Arctic. *Atmos. Chem. Phys.* 15(17), 10057-  
1001 10070, DOI: 10.5194/acp-15-10057-2015.

1002 Samset B. H. & Myhre G. (2011). Vertical dependence of black carbon, sulphate and biomass  
1003 burning aerosol radiative forcing. *Geophys. Res. Lett.* . 38, L24802, DOI: doi:10.1029/2011GL049697.

1004 Samset B. H., Myhre G., Herber A., Kondo Y., Li S. M., Moteki N., Koike M., Oshima N.,  
1005 Schwarz J. P., Balkanski Y., Bauer S. E., Bellouin N., Bernsten T. K., Bian H., Chin M., Diehl T., Easter R.  
1006 C., Ghan S. J., Iversen T., Kirkevåg A., Lamarque J. F., Lin G., Liu X., Penner J. E., Schulz M., Seland Ø.,  
1007 Skeie R. B., Stier P., Takemura T., Tsigaridis K. & Zhang K. (2014). Modelled black carbon radiative  
1008 forcing and atmospheric lifetime in AeroCom Phase II constrained by aircraft observations. *Atmos.*  
1009 *Chem. Phys.* 14(22), 12465-12477, DOI: 10.5194/acp-14-12465-2014.

1010 Samset B. H. & Myhre G. (2015). Climate response to externally mixed black carbon as a  
1011 function of altitude. *Journal of Geophysical Research: Atmospheres*. 120(7), 2913-2927, DOI:  
1012 10.1002/2014JD022849.

1013 Sato Y., Miura H., Yashiro H., Goto D., Takemura T., Tomita H. & Nakajima T. (2016).  
1014 Unrealistically pristine air in the Arctic produced by current global scale models. *Scientific Reports*. 6,  
1015 26561, DOI: 10.1038/srep26561

1016 <http://www.nature.com/articles/srep26561#supplementary-information>.

1017 Schulz M., Textor C., Kinne S., Balkanski Y., Bauer S., Bernsten T., Berglen T., Boucher O.,  
1018 Dentener F., Guibert S., Isaksen I. S. A., Iversen T., Koch D., Kirkevåg A., Liu X., Montanaro V., Myhre  
1019 G., Penner J. E., Pitari G., Reddy S., Seland O., Stier P. & Takemura T. (2006). Radiative forcing by  
1020 aerosols as derived from the AeroCom present-day and pre-industrial simulations. *Atmospheric*  
1021 *Chemistry and Physics*. 6, 5225-5246, DOI: 10.5194/acp-6-5225-2006.

1022 Schwarz J. P., Gao R. S., Spackman J. R., Watts L. A., Thomson D. S., Fahey D. W., Ryerson T.  
1023 B., Peischl J., Holloway J. S., Trainer M., Frost G. J., Baynard T., Lack D. A., de Gouw J. A., Warneke C.  
1024 & Del Negro L. A. (2008). Measurement of the mixing state, mass, and optical size of individual black  
1025 carbon particles in urban and biomass burning emissions. *Geophysical Research Letters*. 35(13), DOI:  
1026 10.1029/2008gl033968.

1027 Schwarz J. P., Samset B. H., Perring A. E., Spackman J. R., Gao R. S., Stier P., Schulz M., Moore  
1028 F. L., Ray E. A. & Fahey D. W. (2013). Global-scale seasonally resolved black carbon vertical profiles  
1029 over the Pacific. *Geophysical Research Letters*. 40(20), 2013GL057775, DOI: 10.1002/2013GL057775.

1030 Seinfeld J. H. & Pandis S. N. (1998), *Atmospheric Chemistry and Physics - From Air Pollution to*  
1031 *Climate Change (2nd edition)*, John Wiley & Sons.

1032 Sharma S., Ishizawa M., Chan D., Lavoué D., Andrews E., Eleftheriadis K. & Maksyutov S.  
1033 (2013). 16-year simulation of Arctic black carbon: Transport, source contribution, and sensitivity  
1034 analysis on deposition. *Journal of Geophysical Research: Atmospheres*. 118(2), 943-964, DOI:  
1035 10.1029/2012JD017774.

1036 Shindell D., Faluvegi G., Walsh M., Anenberg S. C., Van Dingenen R., Muller N. Z., Austin J.,  
1037 Koch D. & Milly G. (2011). Climate, health, agricultural and economic impacts of tighter vehicle-  
1038 emission standards. *Nature Climate Change*. 1(1), 59-66, DOI: 10.1038/nclimate1066.

1039 Shindell D. T., Chin M., Dentener F., Doherty R. M., Faluvegi G., Fiore A. M., Hess P., Koch D.  
1040 M., MacKenzie I. A., Sanderson M. G., Schultz M. G., Schulz M., Stevenson D. S., Teich H., Textor C.,  
1041 Wild O., Bergmann D. J., Bey I., Bian H., Cuvelier C., Duncan B. N., Folberth G., Horowitz L. W., Jonson  
1042 J., Kaminski J. W., Marmer E., Park R., Pringle K. J., Schroeder S., Szopa S., Takemura T., Zeng G.,  
1043 Keating T. J. & Zuber A. (2008). A multi-model assessment of pollution transport to the Arctic.  
1044 *Atmospheric Chemistry and Physics*. 8(17), 5353-5372, DOI: 10.5194/acp-8-5353-2008,.

1045 Shindell D. T., Lamarque J. F., Schulz M., Flanner M., Jiao C., Chin M., Young P. J., Lee Y. H.,  
1046 Rotstajn L., Mahowald N., Milly G., Faluvegi G., Balkanski Y., Collins W. J., Conley A. J., Dalsoren S.,  
1047 Easter R., Ghan S., Horowitz L., Liu X., Myhre G., Nagashima T., Naik V., Rumbold S. T., Skeie R., Sudo  
1048 K., Szopa S., Takemura T., Voulgarakis A., Yoon J. H. & Lo F. (2013). Radiative forcing in the ACCMIP  
1049 historical and future climate simulations. *Atmospheric Chemistry and Physics*. 13(6), 2939-2974, DOI:  
1050 10.5194/acp-13-2939-2013.

1051 Shiraiwa M., Kondo Y., Moteki N., Takegawa N., Miyazaki Y. & Blake D. R. (2007). Evolution of  
1052 mixing state of black carbon in polluted air from Tokyo. *Geophysical Research Letters*. 34(16),  
1053 L16803, DOI: 10.1029/2007gl029819.

1054 Skeie R. B., Berntsen T., Myhre G., Pedersen C. A., Ström J., Gerland S. & Ogren J. A. (2011).  
1055 Black carbon in the atmosphere and snow, from pre-industrial times until present. *Atmospheric*  
1056 *Chemistry and Physics*. 11(14), 6809-6836, DOI: 10.5194/acp-11-6809-2011.

1057 Sovde O. A., Gauss M., Smyshlyaev S. P. & Isaksen I. S. A. (2008). Evaluation of the chemical  
1058 transport model Oslo CTM2 with focus on arctic winter ozone depletion. *Journal of Geophysical*  
1059 *Research-Atmospheres*. 113(D9), D09304, DOI: 10.1029/2007jd009240.

1060 Stjern C. W., Samset B. H., Myhre G., Bian H., Chin M., Davila Y., Dentener F., Emmons L.,  
1061 Flemming J., Haslerud A. S., Henze D., Jonson J. E., Kucsera T., Lund M. T., Schulz M., Sudo K.,  
1062 Takemura T. & Tilmes S. (2016). Global and regional radiative forcing from 20 % reductions in BC, OC  
1063 and SO<sub>4</sub> – an HTAP2 multi-model study. *Atmos. Chem. Phys.* 16(21), 13579-13599, DOI:  
1064 10.5194/acp-16-13579-2016.

1065 Stohl A. (2006). Characteristics of atmospheric transport into the Arctic troposphere. *Journal*  
1066 *of Geophysical Research-Atmospheres*. 111(D11), D11306, DOI: 10.1029/2005jd006888.

1067 Stohl A., Klimont Z., Eckhardt S., Kupiainen K., Shevchenko V. P., Kopeikin V. M. & Novigatsky  
1068 A. N. (2013). Black carbon in the Arctic: the underestimated role of gas flaring and residential  
1069 combustion emissions. *Atmos. Chem. Phys.* 13(17), 8833-8855, DOI: 10.5194/acp-13-8833-2013.

1070 Streets D. G., Bond T. C., Carmichael G. R., Fernandes S. D., Fu Q., He D., Klimont Z., Nelson S.  
1071 M., Tsai N. Y., Wang M. Q., Woo J.-H. & Yarber K. F. (2003). An inventory of gaseous and primary  
1072 aerosol emissions in Asia in the year 2000. *Journal of Geophysical Research*. 108(D21), DOI:  
1073 10.1029/2002JD003093.

1074 Textor C., Schulz M., Guibert S., Kinne S., Balkanski Y., Bauer S., Berntsen T., Berglen T.,  
1075 Boucher O., Chin M., Dentener F., Diehl T., Feichter J., Fillmore D., Ginoux P., Gong S., Grini A.,  
1076 Hendricks J., Horowitz L., Huang P., Isaksen I. S. A., Iversen T., Kloster S., Koch D., Kirkevåg A.,  
1077 Kristjansson J. E., Krol M., Lauer A., Lamarque J. F., Liu X., Montanaro V., Myhre G., Penner J. E., Pitari  
1078 G., Reddy M. S., Seland O., Stier P., Takemura T. & Tie X. (2007). The effect of harmonized emissions  
1079 on aerosol properties in global models - an AeroCom experiment. *Atmospheric Chemistry and*  
1080 *Physics*. 7(17), 4489-4501.

1081 Tiedtke M. (1989). A comprehensive mass flux scheme for cumulus parameterization in  
1082 large-scale models. . *Monthly Weather Review*. 117(8), 1779-1800, DOI: 10.1175/1520-  
1083 0493(1989)117<1779:acmfsf>2.0.co;2.

1084 UNEP/WMO (2011). Integrated assessment of black carbon and tropospheric ozone, 282 pp.,  
1085 United Nations Environmental Programme, Nairobi, Kenya, and World Meteorological Organization,  
1086 Geneva, Switzerland.

1087 van der Werf G. R., Randerson J. T., Giglio L., Collatz G. J., Mu M., Kasibhatla P. S., Morton D.  
1088 C., DeFries R. S., Jin Y. & van Leeuwen T. T. (2010). Global fire emissions and the contribution of  
1089 deforestation, savanna, forest, agricultural, and peat fires (1997–2009). *Atmos. Chem. Phys.* 10(23),  
1090 11707-11735, DOI: 10.5194/acp-10-11707-2010.

1091 Vignati E., Wilson J. & Stier P. (2004). M7: An efficient size-resolved aerosol microphysics  
1092 module for large-scale aerosol transport models. *Journal of Geophysical Research-Atmospheres.*  
1093 109(D22), D22202, DOI: 10.1029/2003jd004485.

1094 Vignati E., Karl M., Krol M., Wilson J., Stier P. & Cavalli F. (2010). Sources of uncertainties in  
1095 modelling black carbon at the global scale. *Atmospheric Chemistry and Physics.* 10(6), 2595-2611,  
1096 DOI: 10.5194/acp-10-2595-2010.

1097 Wang Q., Jacob D. J., Spackman J. R., Perring A. E., Schwarz J. P., Moteki N., Marais E. A., Ge  
1098 C., Wang J. & Barrett S. R. H. (2014). Global budget and radiative forcing of black carbon aerosol:  
1099 Constraints from pole-to-pole (HIPPO) observations across the Pacific. *Journal of Geophysical*  
1100 *Research: Atmospheres.* 119(1), 195-206, DOI: 10.1002/2013JD020824.

1101 Wang T. J., Zhuang B. L., Li S., Liu J., Xie M., Yin C. Q., Zhang Y., Yuan C., Zhu J. L., Ji L. Q. & Han  
1102 Y. (2015). The interactions between anthropogenic aerosols and the East Asian summer monsoon  
1103 using RegCCMS. *Journal of Geophysical Research: Atmospheres.* 120(11), 5602-5621, DOI:  
1104 10.1002/2014JD022877.

1105 Wang X., Doherty S. J. & Huang J. (2013). Black carbon and other light-absorbing impurities  
1106 in snow across Northern China. *Journal of Geophysical Research-Atmospheres.* 118(3), 1471-1492,  
1107 DOI: 10.1029/2012jd018291.

1108 Warneke C., Bahreini R., Brioude J., Brock C. A., de Gouw J. A., Fahey D. W., Froyd K. D.,  
1109 Holloway J. S., Middlebrook A., Miller L., Montzka S., Murphy D. M., Peischl J., Ryerson T. B., Schwarz  
1110 J. P., Spackman J. R. & Veres P. (2009). Biomass burning in Siberia and Kazakhstan as an important  
1111 source for haze over the Alaskan Arctic in April 2008. *Geophysical Research Letters.* 36, L02813, DOI:  
1112 10.1029/2008gl036194.

1113 Warren S. G. & Wiscombe W. J. (1980). A model for the spectral albedo of snow. II: Snow  
1114 containing atmospheric aerosols. *Journal of Atmospheric Sciences.* 37, 2734-2745.

1115 Wesely M. L. (1989). Parameterization of surface resistances to gaseous dry deposition in  
1116 regional-scale numerical models. *Atmospheric Environment (1967).* 23(6), 1293-1304, DOI:  
1117 [http://dx.doi.org/10.1016/0004-6981\(89\)90153-4](http://dx.doi.org/10.1016/0004-6981(89)90153-4).

1118 Wiedinmyer C., Yokelson R. J. & Gullett B. K. (2014). Global Emissions of Trace Gases,  
1119 Particulate Matter, and Hazardous Air Pollutants from Open Burning of Domestic Waste.  
1120 *Environmental Science & Technology.* 48(16), 9523-9530, DOI: 10.1021/es502250z.

1121 Wofsy S. C., Team H. S., Cooperating Modellers T. & Satellite T. (2011). HIAPER Pole-to-Pole  
1122 Observations (HIPPO): fine-grained, global-scale measurements of climatically important atmospheric  
1123 gases and aerosols. *Philosophical Transactions of the Royal Society a-Mathematical Physical and*  
1124 *Engineering Sciences.* 369(1943), 2073-2086, DOI: 10.1098/rsta.2010.0313.

1125 Ye H., Zhang R., Shi J., Huang J., Warren S. G. & Fu Q. (2012). Black carbon in seasonal snow  
1126 across northern Xinjiang in northwestern China. *Environmental Research Letters.* 7(4), 044002, DOI:  
1127 10.1088/1748-9326/7/4/044002.

1128 Zhang Q., Jimenez J. L., Canagaratna M. R., Allan J. D., Coe H., Ulbrich I., Alfarra M. R., Takami  
1129 A., Middlebrook A. M., Sun Y. L., Dzepina K., Dunlea E., Docherty K., DeCarlo P. F., Salcedo D., Onasch  
1130 T., Jayne J. T., Miyoshi T., Shimojo A., Hatakeyama S., Takegawa N., Kondo Y., Schneider J., Drewnick  
1131 F., Borrmann S., Weimer S., Demerjian K., Williams P., Bower K., Bahreini R., Cottrell L., Griffin R. J.,  
1132 Rautiainen J., Sun J. Y., Zhang Y. M. & Worsnop D. R. (2007). Ubiquity and dominance of oxygenated  
1133 species in organic aerosols in anthropogenically-influenced Northern Hemisphere midlatitudes.  
1134 *Geophysical Research Letters.* 34(13), L13801, DOI: 10.1029/2007gl029979.

1135 Zhang X. Y., Wang Y. Q., Niu T., Zhang X. C., Gong S. L., Zhang Y. M. & Sun J. Y. (2012).  
1136 Atmospheric aerosol compositions in China: spatial/temporal variability, chemical signature, regional  
1137 haze distribution and comparison with global models. *Atmos. Chem. Phys.* 12, 779-799.

1138 **TABLES**

1139 *Table 1: Summary and description OsloCTM2-M7 experiments performed in this study.*

| <b>Experiment</b> | <b>Description</b>  |
|-------------------|---|
| Baseline          | Standard M7 OsloCTM2 simulation   |
| CoatThick0.5      | Required coating thickness reduced to 0.5ML                             |
| CoatThick1.4      | Required coating thickness increased to 1.4ML                           |
| CoatThick2.3      | Required coating thickness increased to 2.3ML                           |
| EmisTest          | 50% of biomass burning BC emitted directly in soluble accumulation mode |
| ConvBCi100        | Hydrophobic BC removed by convective precipitation, 100% efficiency     |
| ConvBCi20         | Hydrophobic BC removed by convective precipitation, 20% efficiency      |
| LSice12           | Scavenging by ice in large-scale precipitation reduced from 100% to 20% |
| CombPert          | LCice12 + ConvBCi20   |
| NitCond           | Aging by gas-phase nitric acid condensation included                    |

1140

1141

1142 *Table 2: Global BC lifetime and burden in each experiment.*

|                     | <b>Lifetime</b> | <b>Burden</b> |
|---------------------|-----------------|---------------|
|                     | <b>[days]</b>   | <b>[Gg]</b>   |
| <b>Base</b>         | 6.0             | 133           |
| <b>CoatThick0.5</b> | 4.8             | 106           |
| <b>CoatThick1.4</b> | 6.7             | 150           |
| <b>CoatThick2.3</b> | 8.3             | 185           |
| <b>EmisTest</b>     | 5.9             | 131           |
| <b>ConvBCi100</b>   | 3.6             | 81            |
| <b>ConvBCi20</b>    | 4.8             | 107           |
| <b>LSice12</b>      | 6.6             | 147           |
| <b>Combpert</b>     | 6.6             | 148           |
| <b>NitCond</b>      | 3.9             | 87            |

1143

1144

1145

1146

1147

1148

1149

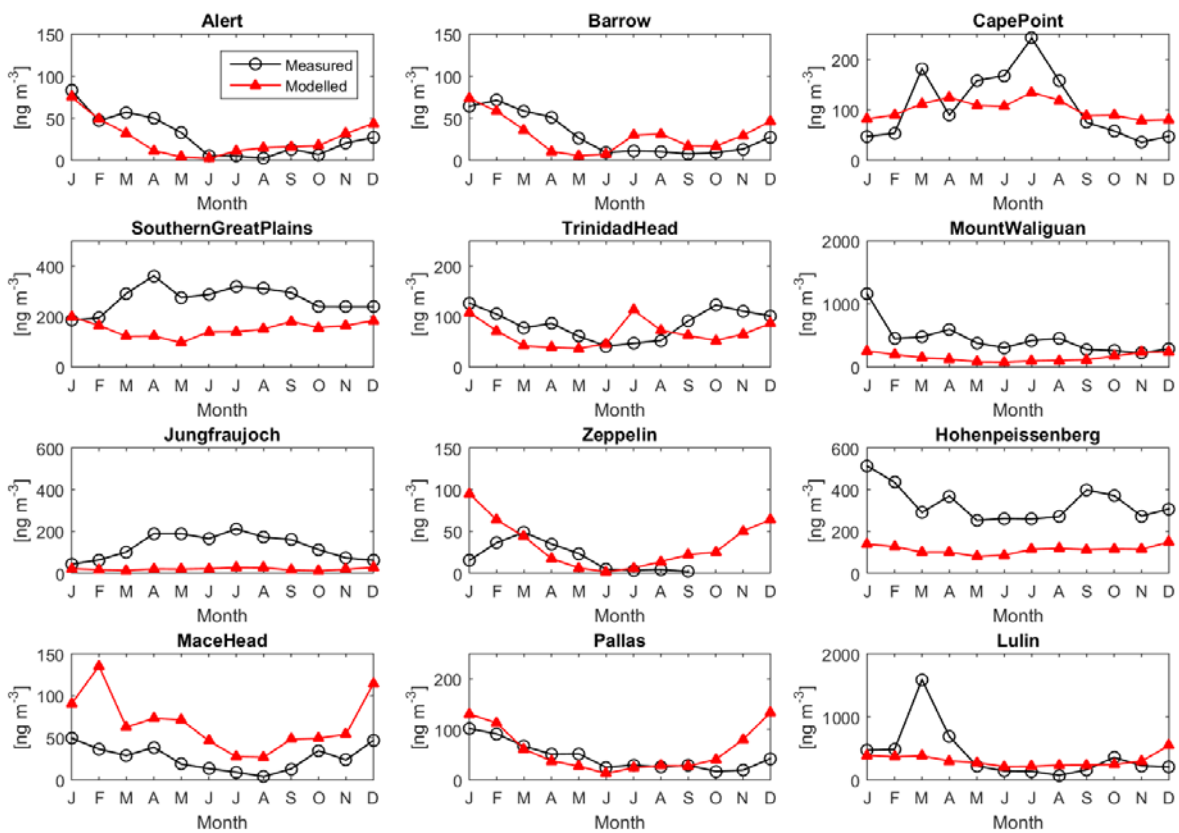
1150

1151

1152

1153 **FIGURES**

1154



1155

1156 *Figure 1: Monthly mean measured EBC versus modelled BC surface concentrations [ $\text{ng}/\text{m}^3$ ]*  
1157 *averaged over 2008-2010 (data at Lulin only available for 2009-2010).*

1158

1159

1160

1161

1162

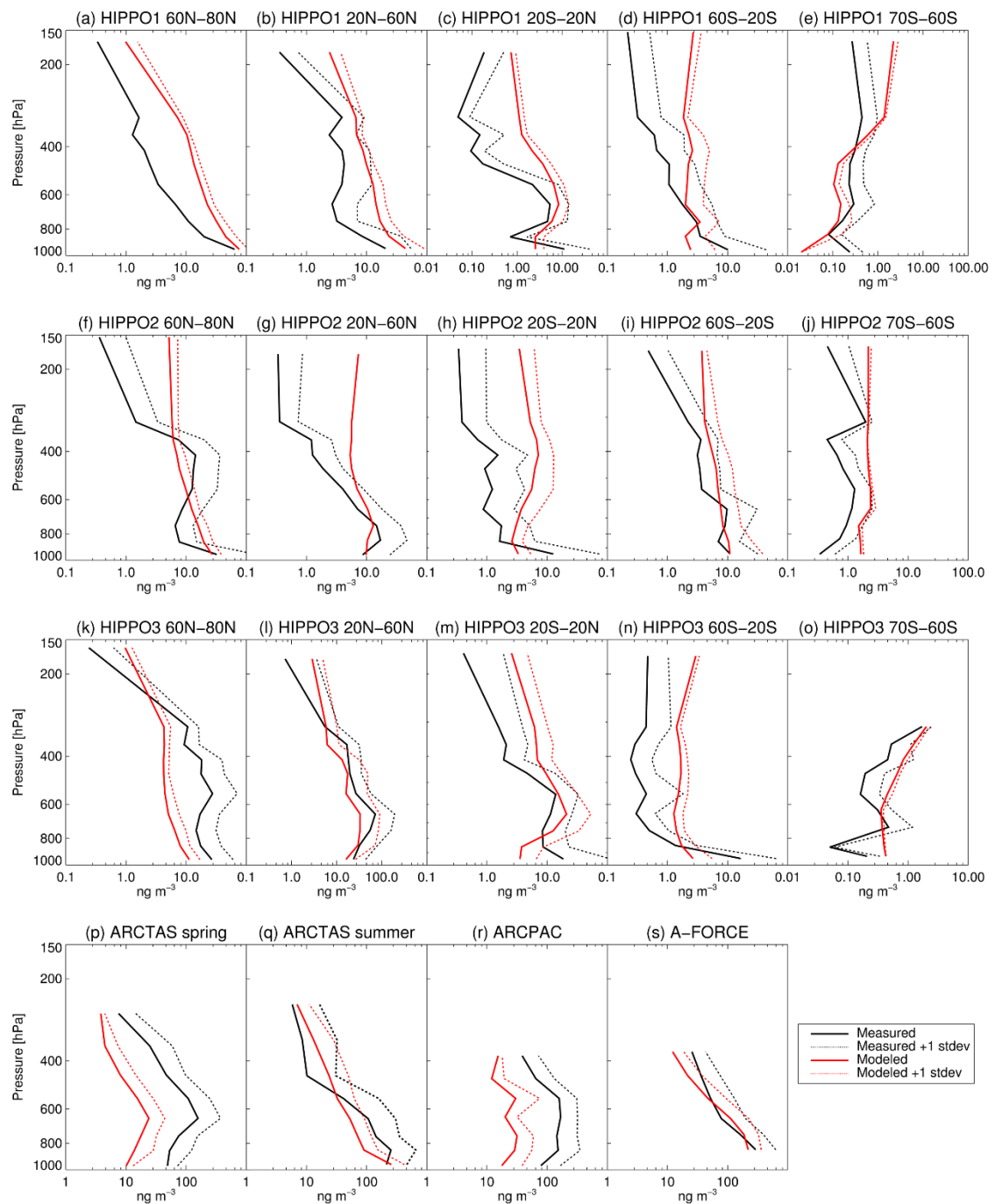
1163

1164

1165

1166

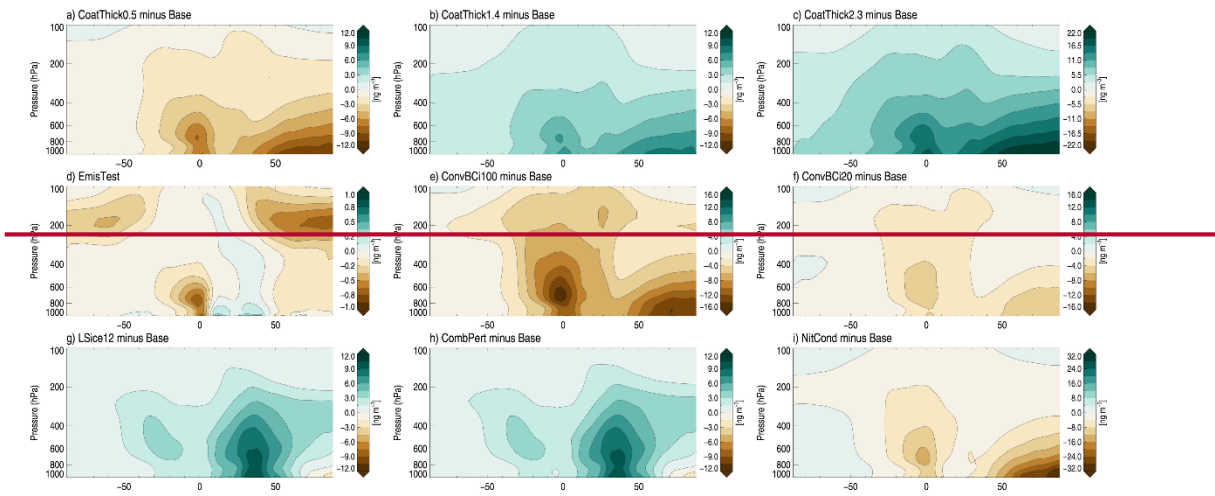
1167



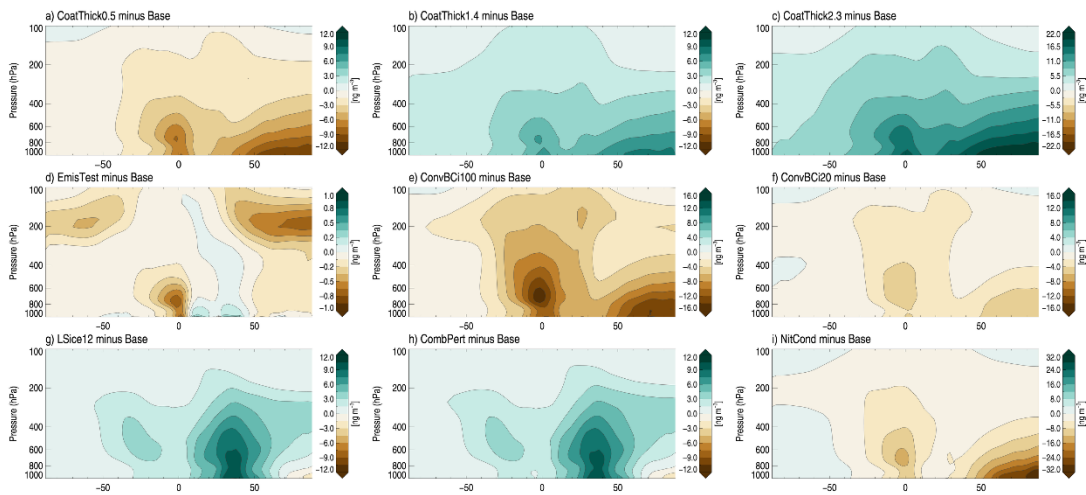
1168

1169 Figure 2: Comparison of modeled vertical profiles of BC with measured rBC from six flight  
 1170 campaigns: (a)-(o) HIPPO 1-3, averaged over five latitude bands, (p)-(q) ARCTAS, spring  
 1171 and summer, (r) ARCPAC and (s) A-FORCE. Solid lines show the average of observations  
 1172 and model results binned in 100 hPa intervals (25 hPa for HIPPO data between 400 and 200  
 1173 hPa), while dashed lines show the standard deviation in each interval.

1174



1175



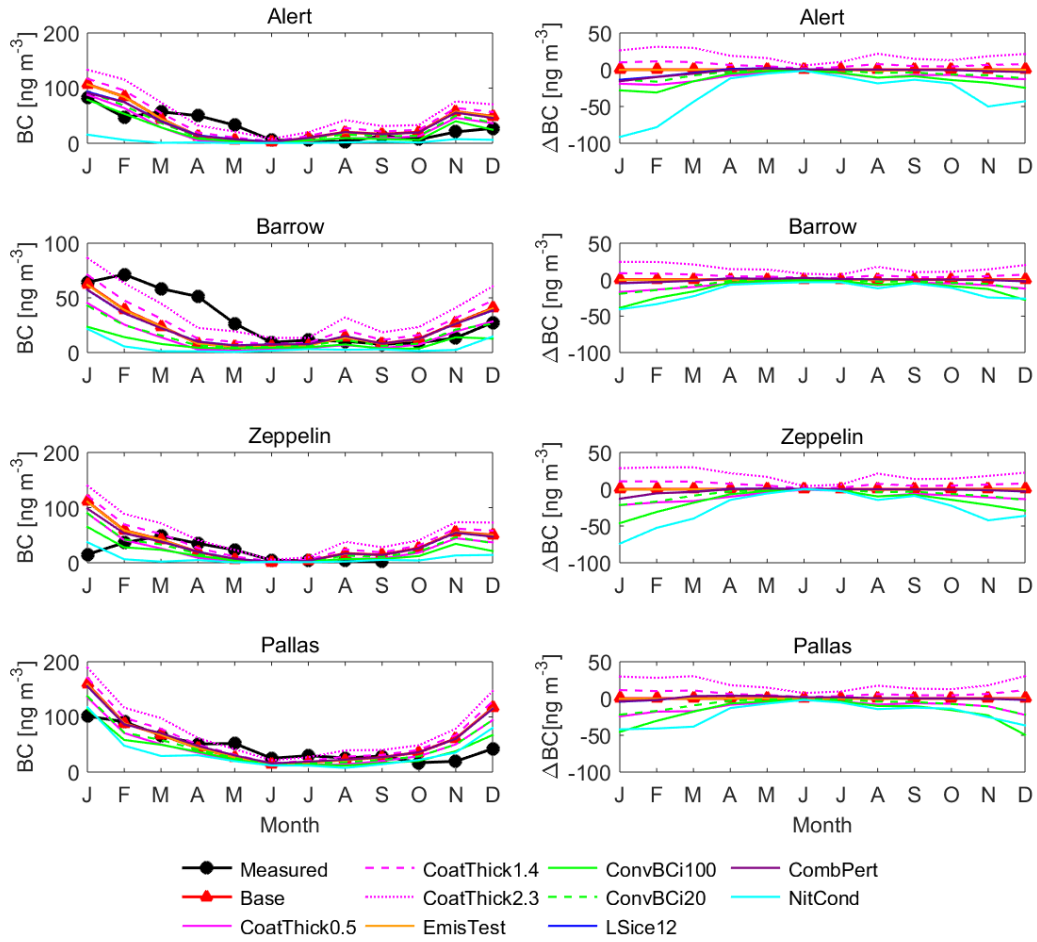
1176

1177 Figure 3: Difference in zonal, annual mean burden [ $\text{ng m}^{-3}$ ] between each sensitivity  
 1178 experiment and the baseline simulation.

1179

1180

1181

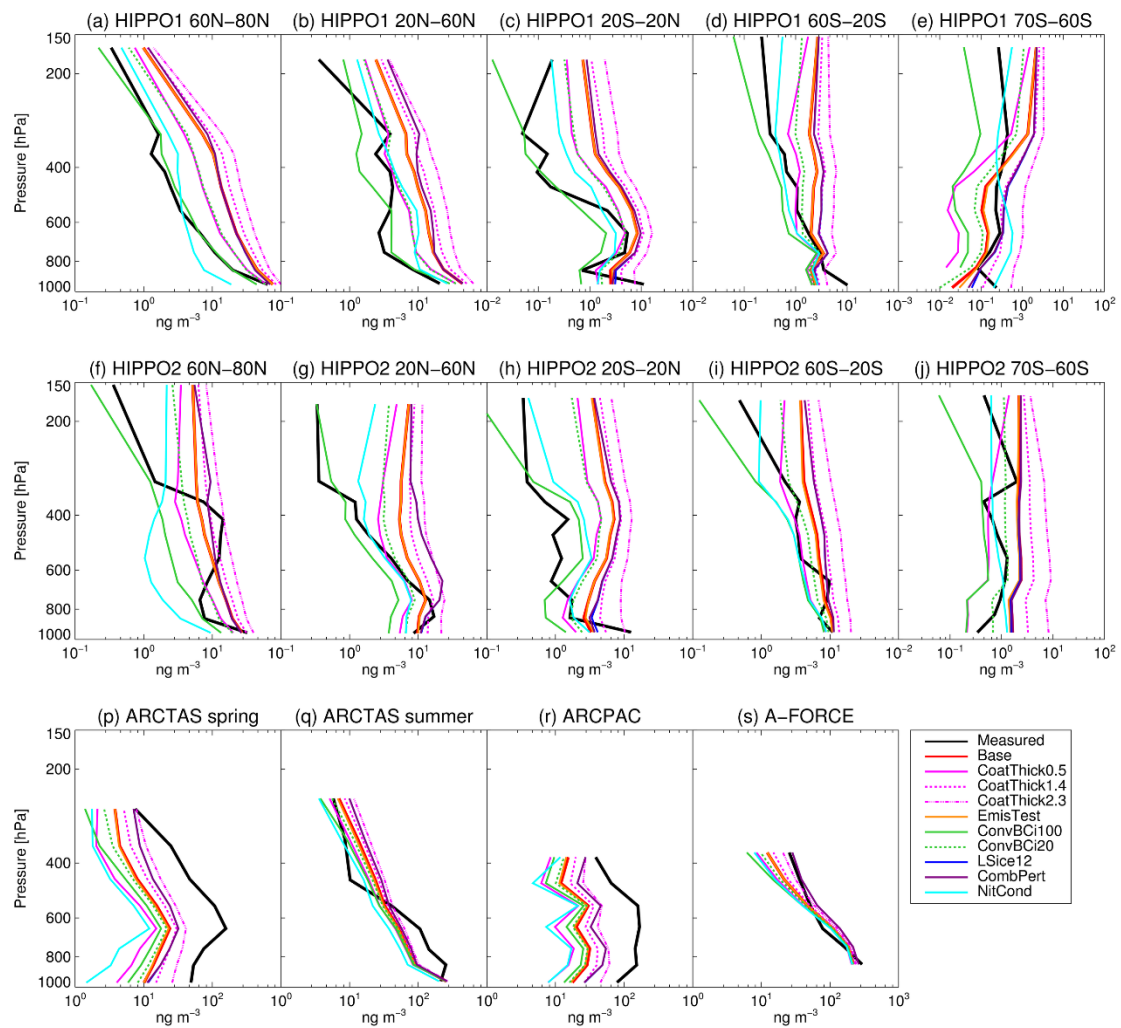


1182

1183 Figure 4: Monthly surface concentrations of BC at Arctic stations in 2008: measurements  
 1184 versus baseline and sensitivity simulations (right column) and difference between each  
 1185 sensitivity simulation and the baseline (left).

1186

1187

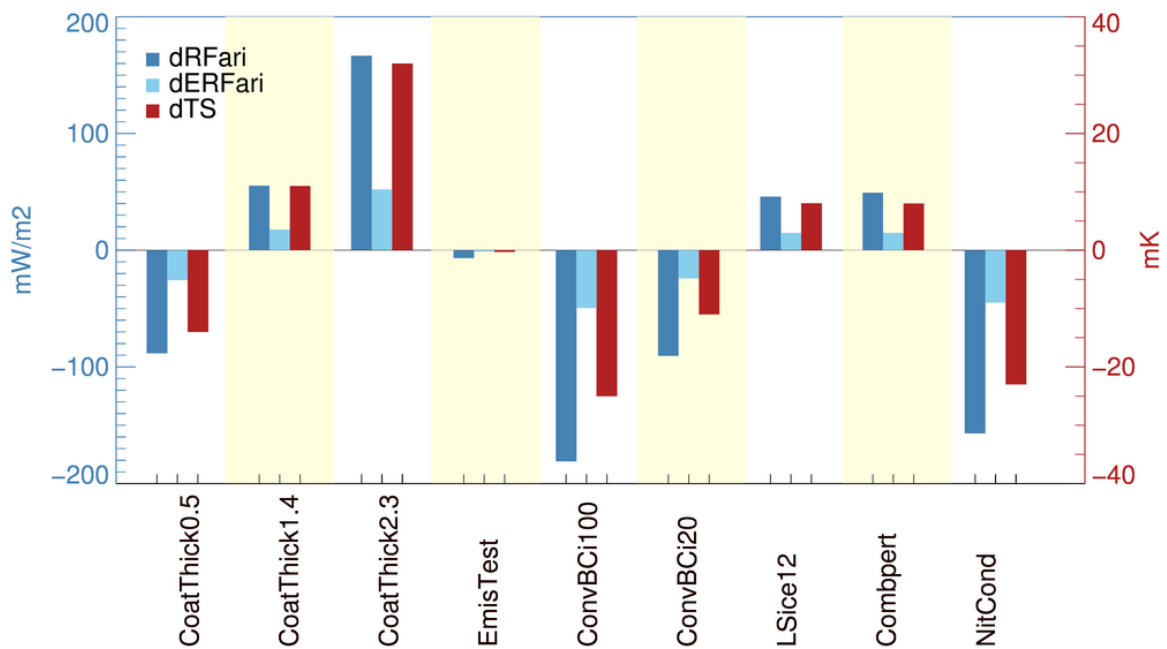


1188

1189 Figure 5: Vertical profiles of BC in the control and sensitivity runs compared to flight  
 1190 campaigns.

1191

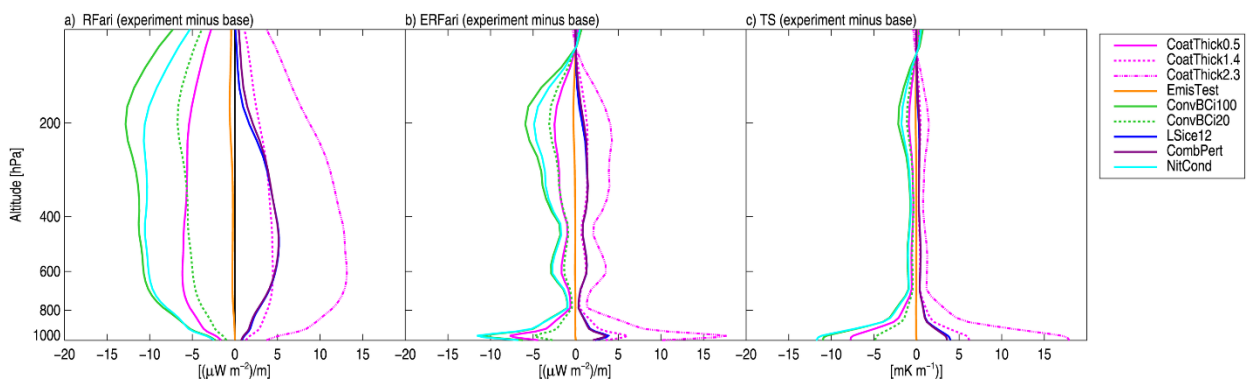
1192



1193

1194 Figure 6: Net change in RFari, ERFari and TS between each sensitivity experiment and the  
 1195 base simulation, estimated using the kernels from (Samset & Myhre, 2015)

1196



1197

1198 Figure 7: Change in a) RFari, b) ERFari and c) TS between each sensitivity experiment and  
 1199 the base simulation as a function of altitude.

1200

1201

1202

1203

1204